CHAPTER 18

Radar Measurements

W. Dale Blair, Mark A. Richards, David A. Long

Chapter Outline

18.1 INTRODUCTION

A radar is designed to transmit electromagnetic energy in a format that permits the extraction of information about the target from its echo. Once a target is detected, the next goal is often to precisely locate that target in three-dimensional space, which requires accurate measurements of the distance and angle (both azimuth and elevation) to the target. In addition, it is often desirable to estimate the radar cross section (RCS) and radial velocity of the target as well.

There are major differences in the way these quantities are measured. The range to the target is measured by estimating the two-way time delay of the transmitted signal. The radial velocity or *range rate* of the target is measured by estimating the Doppler shift in the echo signals. The angular position of the target is measured by comparing signal strength in multiple simultaneous antenna beams offset in angle from one another, obtained either with an antenna structure that forms multiple offset beams (e.g., *monopulse*) or by scanning a single beam across or around the target (e.g., *conical scan*). A radar measures the RCS by using a propagation model (radar range equation) with the measured range and transmitted and received pulse powers to deduce the RCS.

The basic radar range, angle, and radial velocity measurements previously discussed are usually made repeatedly and then combined through kinematic state estimation or filtering of the measurements to produce improved three-dimensional position, velocity, and acceleration estimates, a process called *tracking* the target. The procedures that combine the individual measurements are called *track filtering* algorithms. For closely spaced objects, radar resolution and issues of data association play important roles in the kinematic state estimation, as detections may result from reflected energy from multiple targets and clutter, thermal noise, electromagnetic interference (EMI), and jamming signals from electronic attack sources. Chapter 19 considers how the measurements are combined in the track filtering process.

In this chapter, some of the common techniques for radar measurements are described, along with factors determining their accuracy and precision. Space limitations preclude considering additional techniques and error sources.

18.2 | PRECISION AND ACCURACY IN RADAR MEASUREMENTS

18.2.1 Precision and Accuracy

The quality of the measurement of a single quantity such as position in range or angle is characterized by its *precision* and *accuracy*. Accuracy measures the difference between the measured value and true value. Precision characterizes the repeatability of multiple measurements of the same quantity, even when the accuracy is poor. Thus, accuracy corresponds to the mean error while precision is quantified by the error standard deviation. Figure 18-1 illustrates the difference between these two concepts. Generally, the goal is to minimize both.

In radar, measurement errors are due to a combination of many factors, including interference such as noise and clutter; target phenomenology such as glint and scintillation; signal propagation characteristics such as multipath and turbulence; system measurement limitations such as signal quantization and signal sampling rate; and system uncertainties such as gain calibration, channel-to-channel phase calibration and antenna pointing errors. Error sources can impact both the accuracy and precision of the measurements.

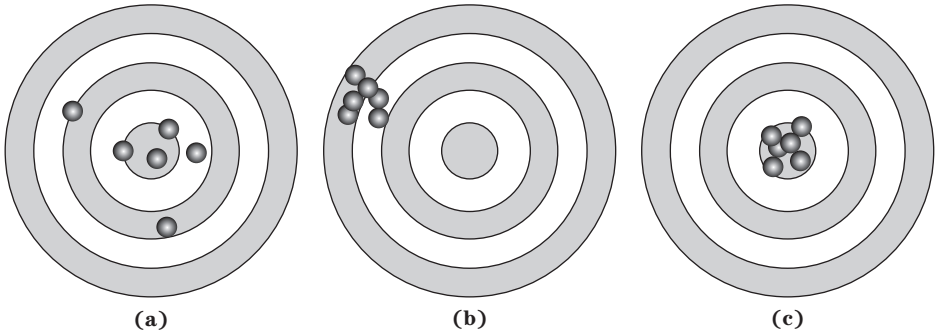

FIGURE 18-1 ■ Illustrating precision and accuracy in target shooting. (a) Accurate but imprecise (low error mean but high standard deviation). (b) Precise but inaccurate (low standard deviation but high mean error). (c) Precise and accurate (low standard deviation and low mean error).

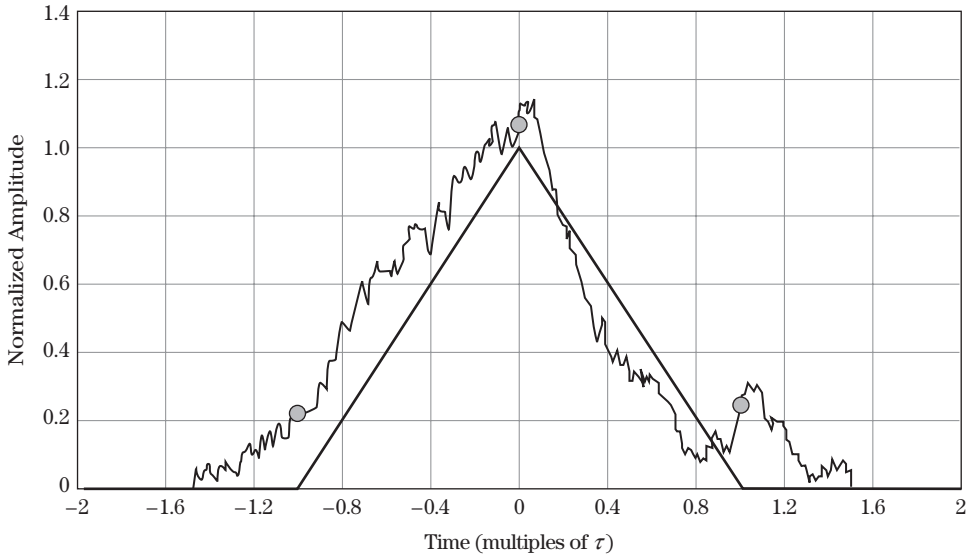

FIGURE 18-2 ■ Noise-free (bold line) and noisy (thin line) matched filter outputs for an ideal rectangular pulse of length τ seconds. The gray circles are samples taken at intervals of τ seconds.

As an example of the effects of noise on the measurement accuracy and precision, consider the output of a matched filter detector for a single simple pulse. In the absence of noise the output is a triangle function (see Chapter 20) as shown in Figure 18-2. Time $t = 0$ corresponds to the delay to the target. In the noise-free case, the time delay of the target echo and thus the range can be measured with no error by locating the peak of the response. A realistic radar, however, must account for the effects of noise and interference. When noise is added to the signal at a signal-to-noise ratio (SNR) of 20 dB, the output peak can be shifted by the noise, as shown in the example. (The gray circles represent samples taken at intervals of τ seconds; these will be discussed later in this chapter.)

Because the interference is random, the error in the peak location is a random variable (RV). If the peak measurement is repeated on noisy data many times, the probability density function (PDF) of that RV can be estimated using a histogram of the measurement data. For example, Figure 18-3a is the histogram of the error for 10,000 trials at an SNR = 20 dB. The mean of the error is the accuracy of the measurement, while the standard deviation is the precision. In this example, the mean of the error is near zero ($-0.0072\ \tau$), so the measurement is very accurate. In this case the accuracy is not dependent of the SNR. However, the range measurement precision does depend on the SNR. As shown in Figure 18-3b, when the SNR is increased, the precision (standard deviation of the error) decreases.

As another example, consider the accuracy and precision of a location angle estimate based on the notional output from the radar receiver for a fixed range bin as the radar system scans past a single, isolated point target. Assume a high pulse repetition frequency, relative to the antenna scan rate, so that the angle samples are closely spaced. In the absence of noise, the measured output voltage is proportional to the two-way antenna voltage pattern, as illustrated in Figure 18-4a for the case of a sinc-squared two-way voltage pattern. The angular position of the target can be accurately determined by simply finding the angle that gives us the peak output power. Thus, the target is located in angle to a precision much better than the angular resolution, which is typically considered to be either the 3 dB or Rayleigh (peak-to-first null) beamwidth of the antenna pattern (one Rayleigh width on the plot).

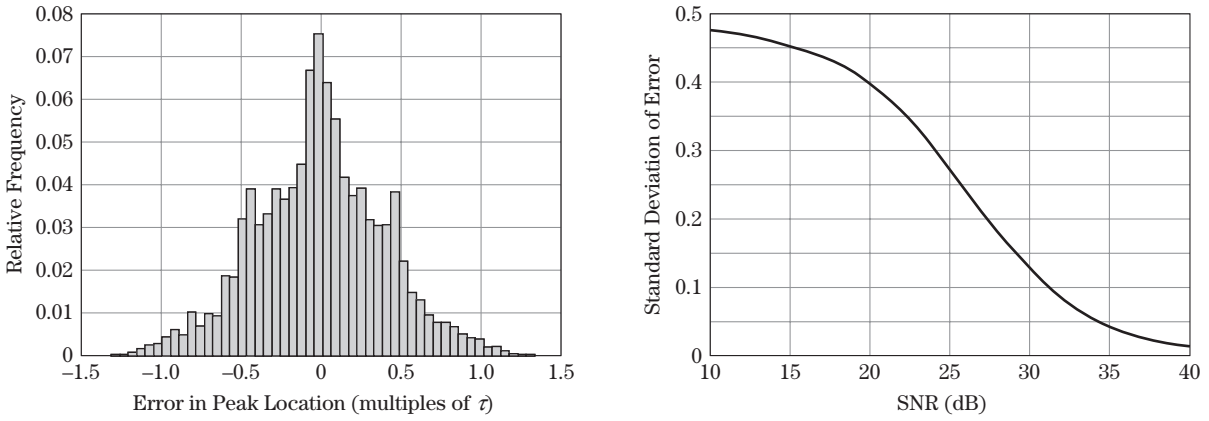

FIGURE 18-3 ■ Statistics of range estimation error using peak detection method. (a) Histogram of peak location measurement error for SNR = 20 dB and 10,000 trials. (b) Standard deviation of error versus SNR.

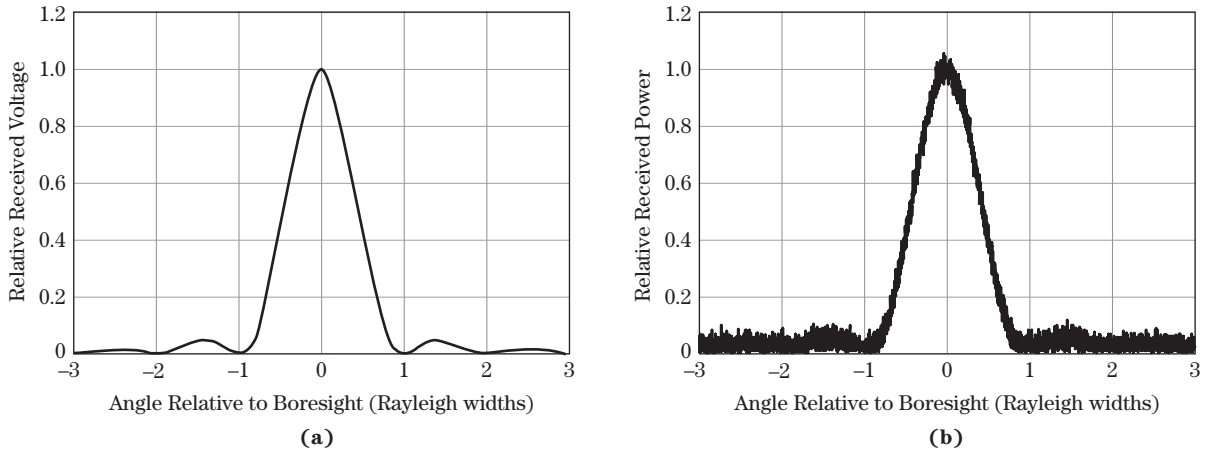

FIGURE 18-4 ■ Received voltage from an angle scan of a single-point target. (a) No noise. (b) 30 dB signal-to-noise ratio.

Now add noise or other interference to the problem. The receiver output now consists of the sum of the target echo, weighted by the antenna pattern, and the noise. The noise may cause the observed peak to occur at an angle other than the true target location, as seen in Figure 18-4b; the actual peak in this sample is at −0.033 Rayleigh widths. As might be imagined, the larger the noise, the greater the likely deviation of the measurement from the noise-free case.

As before, the measured location of the peak receiver output, and thus the estimated angle to the target, is now a random variable. If the peak measurement is repeated on noisy data many times, the probability density function (PDF) of that RV can be estimated using a histogram of the measurement data. Figure 18-5 is an example of the histogram for the observed peak location when additive complex Gaussian noise is included for two values of peak signal-to-noise ratio. The difference between the mean of the PDF of the peak

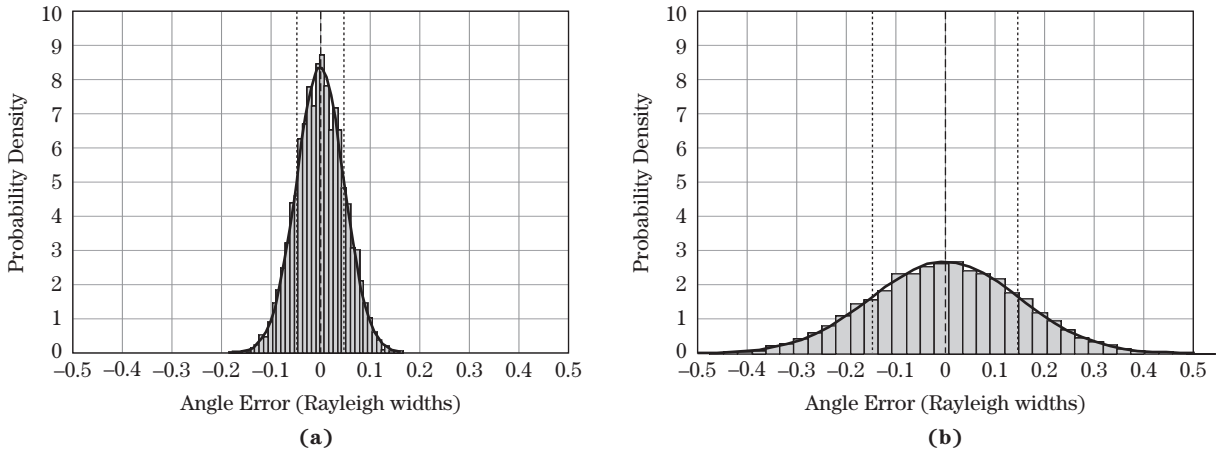

FIGURE 18-5 ■ Histograms of angle error using peak power method. The dark curve is a zero-mean Gaussian PDF with the same variance as the error data. The center dashed line indicates the data mean, with secondary dashed lines at one standard deviation from the mean. (a) 30 dB SNR at boresight. (b) 10 dB SNR at boresight. Note the wider spread (larger standard deviation) of errors at lower SNR.

location and the actual target location is the accuracy of the angle measurement, while the standard deviation of the PDF is the precision of the measurement. In Figure 18-5b, the SNR is 20 dB lower than in 18.5a, a factor of 100. Note that the angle error distribution is wider in the lower SNR case, that is, has a higher variance. In this example, in fact, the variance of the distribution in Figure 18-5b is 9.54 times that of the distribution in Figure 18-5a. This factor is approximately the square root of the 100× change in SNR, suggesting that the variance of the angle estimation error is inversely proportional to the square root of the SNR. The precision is therefore inversely proportional to the fourth root of SNR. On the other hand, the expected value of the error in the peak location is zero for both values of SNR, and hence the accuracy is high and independent of the SNR.

Noise is not the only limitation on measurement quality. Other factors such as resolution and sampling density also come into play. For example, in the angle measurement case, the output power is not measured on a continuous angle axis but only at discrete angles determined by the radar's PRF and the antenna scan rate, resulting in quantization of the angle estimates. Quantization also occurs due to discretized range bins (e.g., the gray circles in Figure 18-2) and arises in sampling and digital signal processing of the signal. Quantization effects can degrade both accuracy and precision; however, consideration of quantization effects is outside of the scope of this chapter. Resolution and sampling density are considered further in Section 18.5.

18.2.2 Accuracy and Performance Considerations

The emphasis in the chapter is on measurement precision. Nevertheless, accuracy considerations are important. Factors affecting measurement accuracy include not only noise and resolution but also signal and target characteristics and radar hardware considerations. For example, any uncertainty in the antenna boresight angle, due for example to mounting or pattern calibration errors or uncertainty, will affect the accuracy of a location measurement. Radiofrequency (RF) hardware or antenna gain calibration errors (gain uncertainty) will affect the accuracy of target signal power measurements. Mismatched in-phase (I) and

quadrature (Q) channels in the receiver can adversely affect both power and phase measurements [1] and may bias range measurements when range compression is used. System timing and frequency error and stability also degrade accuracy. Signal propagation effects are another important factor in overall measurement accuracy: atmospheric refraction of the radar signal and multipath can introduce pointing and range measurement error. All of these effects shift the mean of the parameter measurement, thereby degrading the accuracy.

Because a key source of accuracy degradation is due to error in the values assumed and used for the hardware parameters such as receiver gain, care must be taken to measure or calibrate the system and antenna gain and the antenna pointing angle and beamwidth, for example. The radar design usually includes mechanisms to minimize changes in these parameters. Periodic system calibration is common. One technique is to incorporate a calibration feedback loop wherein an attenuated transmit signal is fed into the antenna or receiver to measure the receiver power from which the system gain can then be inferred. While there is always some residual uncertainty, careful calibration can improve knowledge of the values used in computing signal power, timing, channel-to-channel phase and gain matching, and frequency measurements.

Since there is always residual uncertainty in calibration and knowledge of design parameters, how can the measurement accuracy be estimated? While a detailed treatment of this topic is outside of the scope of this chapter, some comments are provided. A simple, commonly used approach is based on root sum of squares (RSS). The accuracy estimate is computed as the square root of the sum of the squared errors separately determined for each error source. Specifically, given errors $\{\delta_1, \delta_2, \ldots, \delta_N\}$, the RSS estimate of the total error δ is

$$\delta = \sqrt{\delta_1^2 + \delta_1^2 + \ldots \delta_N^2} \tag{18.1}$$

The RSS error effectively treats each error source as independent and Gaussian.

To use RSS, an estimate of the uncertainty of each error source is generated, usually by the system or subsystem designer. For example, suppose that for a particular radar the uncertainty in azimuth boresight pointing angle of the antenna is estimated in testing to be ± 0.03 degrees. This implies that the actual pointing angle is unknown but falls within this range. Alternately, this is the expected range of pointing angle errors for multiple antennas made for the project. Continuing the example, suppose the antenna mounting error is expected to fall in the range of ± 0.05 degrees. The RSS of these values is $\sqrt{(0.03)^2 + (0.05)^2} = 0.058$ degrees.

The RSS technique provides an imperfect, but often reasonably realistic, estimate of the expected pointing error for a particular unit. RSS estimates are popular because they do not require the knowledge of the individual error PDFs needed for more sophisticated error estimation based on signal flow model approaches. Worst-case analysis can also be used and results in a more conservative estimate.

Errors in antenna other estimated parameters such as signal power, the effects of each of the pointing errors on the power are determined. Typically, this is done using nominal values of the radar's operational parameters and the value of the error source is varied. The difference in the power for zero error and values within the range is computed. In the case of antenna pointing errors, the effective antenna gain in the direction of the target is altered. The estimated power difference is the combined effects of other error sources using RSS to yield an estimate of the range of the expected power error (i.e., an error bar for the power measurement accuracy).

Errors in one system parameter also result in errors in other radar measurements. Continuing the example, antenna pointing errors alter the antenna gain in the direction of a target, in turn altering the received echo power. Typically, the effect of each source of pointing error on the power is determined by assuming the nominal values of the radar's other operational parameters (e.g., transmitted power, system losses) and varying one source of pointing error to estimate the resulting variation in received power. The power variances due to each identified error source are combined using the RSS technique to provide an estimate of the range of the expected power error.

18.3 | RADAR SIGNAL MODEL

The radar range equations presented in earlier chapters of this book are expressions of average power or energy and are often used for system-level trade studies in radar system design and analysis. However, radar measurements are typically formed with the voltage signals. Thus, the voltage form of the radar signals is used for the modeling and analysis of radar measurements for tracking studies. Since voltage is proportional to the square root of power, a general model of the RF echo signal received in the radar, for either a conventional antenna or the sum channel of a monopulse from a single target, can be written as

$$s(t) = 2\sqrt{\frac{P_t}{(4\pi)^3}}\frac{\lambda}{R^2}\xi V_\Sigma^2(\theta, \psi)\, p(t)\cos(\omega_c t + \omega_d t + \phi) + w_\Sigma(t) \tag{18.2}$$

where

P_t = transmitted power.
λ = wavelength.
R = range to target.
ξ = voltage reflectivity of the target.
$G_\Sigma(\theta, \psi)$ = voltage gain of the antenna at the angles (θ, ψ).
(θ, ψ) = angular location of the target relative to antenna boresight.
$p(t)$ = envelope of the matched filter output for the transmitted pulse.
ω_c = carrier frequency of the transmitted waveform.
ω_d = Doppler shift of the received waveform.
ϕ = phase of the target echo.
$w_\Sigma(t)$ = receiver noise.

The "voltage reflectivity," ξ, of the target is related to its RCS σ according to

$$\sigma = \xi^2/2 \tag{18.3}$$

Note that in equation (18.2) the normalized antenna voltage gain pattern $V_\Sigma(\theta, \psi)$ is assumed to be the same on transmit and receive, so the two-way pattern is $V_\Sigma^2(\theta, \psi)$ as shown. The antenna gain pattern is assumed to be the product of two orthogonal voltage patterns,

$$V_\Sigma(\theta, \psi) = W(\theta)U(\psi) \tag{18.4}$$

where $W(\theta)$ and $U(\psi)$ are the elevation and azimuth voltage patterns, respectively.

Demodulation by coherent mixing with quadrature oscillators at the frequency ω_c removes the carrier term of equation (18.2), as described in Chapter 11. Two common sources of error frequently reduce the measured amplitude of the signal $s(t)$. First, if $s(t)$ is mixed with ω_c rather than $\omega_c + \omega_d$, a frequency mismatch occurs in the matched filter for $p(t)$, resulting in a loss in SNR referred to as *Doppler loss*, as discussed in [2,4] and in Chapter 20. When attempting to use a radar system designed for air targets to detect and track space targets traveling at significantly higher velocity, the Doppler loss can be sufficiently high to prevent detection. Second, the need to detect targets at a priori unknown ranges and to detect multiple, closely spaced objects in the same dwell dictates that the output of the matched filter be sampled periodically in fast time at the bandwidth of the signal over the range interval (*range window*) of interest. There is no guarantee that one of the samples will fall on the peak of the matched filter response, as seen in the example in Figure 18-2. Instead, the energy of a target echo may be captured in adjacent samples that straddle the peak, reducing the measured SNR. This reduction in SNR is often referred to as *straddle loss*. However, as will be seen, the signals in the adjacent cells can be used to improve the range estimate precision beyond the resolution and to reduce straddle loss.

Ignoring any Doppler and straddle losses, the I and Q components of the sampled output of the matched filter with gain p_0 are given by

$$s_I = \alpha \cos\phi + w_{\Sigma I} \quad s_Q = \alpha \sin\phi + w_{\Sigma Q} \tag{18.5}$$

where

$$\alpha = \frac{\sqrt{P_t}}{(4\pi)^{3/2}} \frac{\lambda}{R^2} \xi V_\Sigma^2(\theta, \psi) p_0, \quad w_{\Sigma I} \sim \mathrm{N}\big(0, \sigma_\Sigma^2/2\big), \quad w_{\Sigma Q} \sim \mathrm{N}\big(0, \sigma_\Sigma^2/2\big) \tag{18.6}$$

where

p_0 = pulse amplitude.
$\sigma_\Sigma^2 = kT_0F_nB_{IF}$ = total noise power at the receiver output.
k = Boltzmann's constant.
$T_0 = 290\ ^\circ\mathrm{K}$ = standard noise temperature.
F_n = receiver noise figure.
B_{IF} = receiver intermediate frequency bandwidth.

The other variables are as given previously, and the notation $\sim\mathrm{N}(0, \sigma^2)$ indicates a normally distributed (Gaussian) random variable with zero mean and a variance of σ^2. Any gain due to coherent integration such as pulse compression, moving target indication (MTI), or pulse-Doppler processing with a discrete Fourier transform (DFT) is included in s_I and s_Q. The integration of s_I and s_Q from multiple pulses after pulse compression and Doppler processing is typically accomplished using only the measured amplitude of the pulses, ignoring the phase, and is referred to as *noncoherent integration*. Often, channel-dependent calibration corrections for gain, time delay, and phase shift are also applied to the measured values to improve their accuracy.

Letting Λ and φ denote the measured amplitude and phase of the signals in equation (18.5), including the calibration corrections and noise contributions, gives

$$s_I = \Lambda \cos\varphi, \quad s_Q = \Lambda \sin\varphi \tag{18.7}$$

It is useful to define the *observed SNR* as the ratio of total signal power to total noise power

$$SNR_{\text{obs}} = \frac{\Lambda^2}{\sigma_\Sigma^2} \tag{18.8}$$

Λ includes both signal and noise contributions, so SNR_{obs} is actually a signal-plus-noise-to-noise ratio. The SNR of a target can therefore be computed for the expected value of the observed SNR, that is,

$$SNR = \text{E}\{SNR_{\text{obs}}\} - 1 \tag{18.9}$$

where $\text{E}\{\cdot\}$ denotes the expected value.

18.4 PARAMETER ESTIMATION

The goal of the radar measurement process is to estimate the various parameters of the target reflected in the signal $s(t)$. The primary parameters of interest include the reflectivity amplitude, ξ, the Doppler shift, ω_d, the angular direction to the target, (θ, ψ), and the time delay to the target, which is reflected in the sampling time at which the signal was measured and in the signal phase, ϕ. Before addressing techniques for measuring each of these, it is useful to first discuss the general idea of an *estimator* and the achievable precision.

18.4.1 Estimators

Consider an observed signal $y(t)$ that is the sum of a target component $s(t)$ and a noise component $w(t)$:

$$y(t) = s(t) + w(t) \tag{18.10}$$

The signal $y(t)$ is a function of one or more parameters θ_i. These might be, for example, the time delay, amplitude, Doppler shift, or angle of arrival (AOA) of the target component. The goal is to estimate the parameter values given a set of observations of $y(t)$. This is done using an *estimator*.

Suppose $y(t)$ is sampled multiple times (intrapulse or over multiple pulses) to produce a vector of N observations,

$$\mathbf{y} = \{y_1, y_2, \ldots y_N\} \tag{18.11}$$

Because of the noise, the data $\mathbf{y}$ is a random vector that depends on the parameter θ. Thus, $\mathbf{y}$ is described by a conditional PDF $p(\mathbf{y}|\theta)$. Now define an estimator f of a parameter θ based on the data $\mathbf{y}$,

$$\hat{\theta} = f(\mathbf{y}) \tag{18.12}$$

Because $\mathbf{y}$ is random, the estimate $\hat{\theta}$ is also a random variable and therefore has a probability density function with a mean and variance.

Two desirable properties of an estimator are that it be *unbiased* and *consistent*. These mean that the expected value of the estimate equals the actual value of the parameter, and that the variance of the estimate decreases to zero as more measurements become available:

$$\begin{aligned} &\mathbf{E}\{\hat{\theta}\} = \theta_i && \text{(unbiased)} \\ &\lim_{N\to\infty} \left\{\sigma_{\hat{\theta}}^2\right\} \to 0 && \text{(consistent)} \end{aligned} \tag{18.13}$$

In other words, a desirable estimator produces estimates that are, on average, accurate and whose precision improves with more data.

A simple example of a good estimator is one that estimates the value of a constant signal A in the presence of white (and thus zero-mean) noise $w[n]$ of variance σ_w^2 by averaging N samples of the noisy signal $y[n] = A + w[n]$. In this case, the parameter θ is the unknown amplitude A, the vector $\mathbf{y}$ is composed of the N samples of $y[n]$, and the estimator is

$$\begin{aligned}\hat{A} &= f(\mathbf{y}) = \frac{1}{N}\sum_{n=0}^{N-1} y[n] \\ &= \frac{1}{N}\sum_{n=0}^{N-1} (A + w[n]) = A + \frac{1}{N}\sum_{n=0}^{N-1} w[n] \end{aligned} \tag{18.14}$$

Note that the expected value of $\hat{A} = A$, so the estimator is unbiased. The variance of the second (noise) term is σ_w^2/N; this is also the variance of $\hat{A}$. Thus, the variance of the estimator tends to zero as the number of data samples increases, so it is also consistent. The expected value of the square root of the variance (the standard deviation) of the estimate is the measurement precision.

The absolute value of the variance of the estimate is less significant than its value relative to the value of A. Normalizing the estimator variance by the signal power A^2 gives the normalized measurement variance

$$\frac{\sigma_w^2}{NA^2} = \frac{1}{N \cdot SNR} \tag{18.15}$$

where the SNR for this problem is A^2/σ_w^2. The normalized estimate variance is thus an example of an estimator whose variance is inversely proportional to the SNR.

Many types of estimators exist. Two of the most commonly used are *minimum variance* (MV) estimators and *maximum likelihood* (ML) estimators. A minimum variance or minimum variance unbiased (MVU) estimator is one that is both unbiased and minimizes the mean square error between the actual value of the parameter being estimated and its estimate [3]. In the context of this chapter, it minimizes $(\hat{\theta} - \theta)^2$ under the condition that $\mathrm{E}\{\hat{\theta}\} = 0$.

The maximum likelihood estimator is one that chooses $\hat{\theta}$ to maximize the likelihood of the specific observed data values $\mathbf{y}$. For example, suppose an observed signal sample, s, is assumed to be the sum of a constant value, A, and zero-mean Gaussian noise of variance, σ^2. The observation s is then Gaussian with mean A and variance σ^2, $s \sim \mathrm{N}(A, \sigma^2)$. The goal is to estimate the mean. For concreteness, suppose $A = 3$ and $\sigma^2 = 1$, and a single measurement results in the observed value $s = 2.8$. The ML estimate of A based on s is $\hat{A}_{ML} = 2.8$ because that is the value of the Gaussian mean that maximizes the chance that the measured value is 2.8. As will be seen later, if multiple measurements of s are available, the ML estimator of A is the sample mean.

The ML estimator is often a good practical choice because its form is often relatively easy to determine. In addition, in the case of Gaussian noise it is equivalent to the MV estimator and thus is the optimum estimator.

As previously noted the standard deviation of the estimate error describes the measurement precision. The standard deviation depends on the estimator chosen, and sometimes can be hard to compute for a particular estimator. However, as described in the following section, the error standard deviation can be bounded.

18.4.2 The Cramèr-Rao Lower Bound

In the angle measurement example in Section 18.2.1, it was seen that the variance of the angle estimate decreased with increasing SNR. Similar behavior is typically observed for range and Doppler estimates as well. Specifically, for a parameter θ, the variance $\sigma_{\hat{\theta}}^2$ of the estimated value $\hat{\theta}$ often behaves as

$$\sigma_{\hat{\theta}}^2 = \frac{k}{SNR} \tag{18.16}$$

for some constant k. Is this behavior predictable and, if so, what can be said about the constant k?

The *Cramèr-Rao lower bound* (CRLB) is a famous result that addresses these questions. The CRLB, $J(\theta)$, establishes the minimum achievable variance (square of precision) of an unbiased estimator of the parameter θ. The square root of the CRLB is thus the best achievable precision. Any particular unbiased estimator must have a variance equal to or greater than the CRLB, and the quality of a particular estimator can be judged by how close its actual variance comes to achieving the CRLB.

An important metric for describing an estimator's performance is the *root mean square* (RMS) *error*. For zero-mean error the square root of the CRLB is the minimum achievable RMS error. While the CRLB does not depend on the estimator, the RMS error is a function of the estimator employed.

Derivation of the CRLB is beyond the scope of this chapter; good (and very similar) derivations are given in [3,4]. The bound states that the minimum variance in the estimate $\hat{\theta}$ is

$$\sigma_{\hat{\theta}}^2 \geq J(\theta) = \frac{1}{\mathbf{E}\left[\{\partial \ln\{p(\mathbf{y}|\theta)\}/\partial\theta\}^2\right]} \tag{18.17}$$

where $p(\mathbf{y}|\theta)$ is the conditional probability density function (PDF) of the data vector $\mathbf{y}$ given some particular value of the parameter θ. Under some mild conditions, the CRLB has an alternate form,

$$\sigma_{\hat{\theta}}^2 \geq J(\theta) = \frac{-1}{\mathbf{E}\left[\partial^2 \ln\{p(\mathbf{y}|\theta)\}/\partial\theta^2\right]} \tag{18.18}$$

The choice between equation (18.17) or (18.18) is a matter of convenience, depending on the functional form of $\ln\{p(\mathbf{y}|\theta)\}$. More general forms of the CRLB that include bias are possible [3,4].

The CRLB can be further simplified for the special but very common and important case of a signal in additive Gaussian noise. Suppose the data $\mathbf{y}$ is N observations of a real discrete signal s that is a function of some parameter θ in real white Gaussian noise,

$$y[n] = s[n;\theta] + w[n], \quad n = 0, \ldots, N-1, \quad w[n] \sim \mathrm{N}\left(0, \sigma_w^2\right) \tag{18.19}$$

Starting from equation (18.18), it can be shown that for this case the CRLB is [3]

$$J(\theta) = \frac{\sigma_w^2}{\sum_{n=0}^{N-1} \left(\frac{\partial s[n;\theta]}{\partial\theta}\right)^2} \tag{18.20}$$

It is sometimes more convenient to deal with continuous time rather than sampled signals. The continuous time equivalents to equations (18.19) and (18.20) are

$$y(t) = s(t;\theta) + w(t), \quad -T/2 \le t \le T/2, \quad w(t) \sim \mathrm{N}\left(0, \sigma_w^2\right) \tag{18.21}$$

$$J(\theta) = \frac{\sigma_w^2}{\int\limits_{t=-T/2}^{T/2} \left(\frac{\partial s(t;\theta)}{\partial \theta}\right)^2 dt} \tag{18.22}$$

where T is the duration of the signal of interest.

As a simple illustration of equation (18.20), consider estimating the value of a constant m in Gaussian noise. In this case, $s[n;\theta] = m$, so $\partial s[n;\theta]/\partial\theta = \partial(m)/\partial m = 1$ and the CRLB for estimating m becomes

$$J(\theta) = J(\hat{m}) = \frac{\sigma_w^2}{N}, \tag{18.23}$$

which is achieved for the mean estimator in equation 18.14 and shows that, as expected, the minimum achievable variance of the estimate decreases with the number of measurements available. A better metric than the variance in $\hat{m}$ is the variance normalized to the actual signal power m^2, *i.e.* the relative error. The CRLB for this quantity is

$$J\left(\frac{\hat{m}}{m}\right) = \frac{\sigma_w^2}{N \cdot m^2} = \frac{1}{N \cdot SNR} \tag{18.24}$$

Notice that the CRLB of the normalized error estimate varies as 1/*SNR*. This proves to be the case in many radar parameter estimation problems.

18.4.3 Precision and Resolution for the Gaussian Case

Equation (18.20) states that the minimum achievable precision of a measurement increases as the square of the derivative of the signal with respect to the parameter of interest increases. Loosely interpreted, the more rapidly the signal varies, the better the precision. For example, if the parameter of interest is range, then a matched filter output with a steep leading and trailing edge will allow better range measurement precision than a broad, slowly rising and falling output waveform. Similarly, a narrow antenna mainlobe should allow better angular precision than a wide one. This should not seem surprising. A waveform with sharp edges suggests a high bandwidth in the dimension of interest: temporal bandwidth in time or range or spatial bandwidth in angle. Thus, it might be anticipated that higher bandwidths lead to lower CRLBs, at least in the Gaussian noise case.

This is in fact the case. As an example, consider time-delay estimation. The parameter θ in equation (18.20) is then the time delay, t_0, of the signal echo, and the signal itself is

$$s[n;\theta] = s[nT_s - t_0] \tag{18.25}$$

where T_s is the sampling interval in fast time. Using equation (18.25) in (18.20), several references [3–5] derive the result that

$$\sigma_{t_0}^2 \ge J(t_0) = \frac{2E}{N_0} \cdot \frac{1}{B_{rms}^2} \tag{18.26}$$

where E is the energy in the signal s, N_0 is the noise power spectral density, and B_{rms} is the *RMS bandwidth* of s, defined as

$$B_{rms} = \sqrt{\frac{\int_{-\infty}^{\infty} (2\pi f)^2 |S(f)|^2 \, df}{\int_{-\infty}^{\infty} |S(f)|^2 df}} \tag{18.27}$$

where $S(f)$ is the Fourier transform of $s(t)$.

B_{rms} is the square root of the normalized variance of $|S(f)|^2$. It is proportional to other more common measures of bandwidth, such as the 3 dB or Rayleigh bandwidths. For example, if $S(f)$ is a rectangular spectrum of width B Hz, then $B_{rms} = \pi/\sqrt{3} \cdot B \approx 1.81\, B$.

Similarly, the *RMS time duration,* τ_{rms}, is defined as

$$\tau_{rms} = \sqrt{\frac{\int_{-\infty}^{\infty} t^2 |s(t)|^2 \, dt}{\int_{-\infty}^{\infty} |s(t)|^2 \, dt}} \tag{18.28}$$

Following a procedure similar to that used to derive $J(t_0)$, it can be shown that the Doppler frequency estimate CRLB obeys [4]

$$\sigma_{\omega_d}^2 \geq J(\omega_d) = \frac{2E}{N_0} \cdot \frac{1}{\tau_{rms}^2} \tag{18.29}$$

The term $2E/N_0$ in equations (18.26) and (18.29) is recognized as the peak SNR at the output of a matched filter (Chapter 20 or [1]), so that those two equations can be rewritten as

$$\sigma_{t_0}^2 \geq \frac{1}{SNR \cdot B_{rms}^2} \tag{18.30}$$

$$\sigma_{\omega_d}^2 \geq \frac{1}{SNR \cdot \tau_{rms}^2} \tag{18.31}$$

Equation (18.30) shows that the time-delay estimation variance improves with both SNR and bandwidth. Since range is related to time delay by $R = ct/2$, this result can also be scaled and the square root taken to provide the range precision,

$$\sigma_R \geq \frac{c}{2\sqrt{SNR} \cdot B_{rms}} \tag{18.32}$$

Finally, recalling that range resolution is generally of the form $\Delta R = c/2B$, where B is an appropriate bandwidth, the range precision can be expressed as

$$\sigma_R \geq \frac{\Delta R}{\sqrt{SNR}} \tag{18.33}$$

Equation (18.33) shows that range estimation precision generally improves with finer-range resolution as well as with SNR. In fact, since $SNR > 1$ (and often $SNR \gg 1$) in any realistic detection scenario, this equation suggests that the lower bound on precision can be a small fraction of the resolution, as was seen in the first few examples in this chapter.

For instance, if $SNR = 10$ (10 dB), the lower bound on precision above is 32% of the RMS range resolution; if it is 100 (20 dB), the bound is 10% of the RMS resolution. In many practical systems, however, system limitations and signal variability create additional limits on estimation precision.

18.4.4 Signal and Target Variability

The derivations presented in the previous sections are based on the assumption that the target and signal characteristics remain stationary over the time period required to collect the samples. If the target characteristics or the signal propagation conditions vary over the sampling period, *signal variability* is introduced, which increases the estimate variation and thus degrades the measurement precision. A major source of target variability is changes in the target aspect angle that cause *scintillation* (exponentially distributed fluctuations of the target RCS as described in Chapter 15) and glint. *Glint* is a fluctuation of the apparent angle of the target relative to the radar boresight caused by variations in the orientation of the phase front of the echo signal at the antenna, possibly due to changes in the scattering location on the target. Multipath and diffraction in the signal path can also introduce signal fluctuation as well as possible multiple apparent targets.

If appropriate models for signal and target variability are available, these can be included in the probability density function used in deriving measurement estimators and computing the CRLB. In the interest of clarity and brevity, only a few specific Swerling cases for signal and target variability are considered in this chapter.

18.5 RANGE MEASUREMENTS

The previous discussion considered range measurement precision. Additional methods and accuracy analyses are provided in this section after a discussion on the effects of resolution and sampling. Note that although the discussion on resolution and sampling focuses on range and angle measurement, these issues also impact phase and Doppler measurement.

18.5.1 Resolution and Sampling

A typical radar collects target returns for each transmitted pulse over some finite time-delay interval or *range window*. The start of the range window may be positioned at any range beyond the blind range of the radar. The output of the matched filter is sampled periodically over the range window, usually at a spacing equal to the bandwidth of the waveform but sometimes at higher rates, for example, in a dedicated tracking mode. Thus, the time delay or range estimation is accomplished with a sequence of periodic samples of the matched filter output.

The range resolution of the radar can be generally expressed as (see Chapter 20)

$$\Delta R = \alpha \frac{c}{2B} \tag{18.34}$$

where B is the waveform bandwidth, and α is a factor in the range $1 < \alpha < 2$ that represents the degradation in range resolution resulting from system errors or range sidelobe reduction techniques such as windowing. The bandwidth, B/α, corresponds to the bandwidth of the

intermediate frequency (IF) filter and defines the Nyquist sampling rate at the output of the matched filter unless some technique such as stretch processing as discussed in [1] is employed.

Most radars sample the receiver output at a rate of approximately 1 to 1.5 samples per 3 dB resolution cell in range and angle. For a simple pulse waveform, $B \approx 1/\tau$ so that the matched filter output of Figure 18-2 would be sampled approximately every τ seconds. Figure 18-2 illustrated this sampling strategy. Depending on the alignment of the target's actual range with the sampling times, only two to three samples may be taken on the response to a single-point target. This sparse set of measurements must be used to estimate the peak location. The coarsely time-quantized nature of the sampling contributes to variability in the resulting estimates. In contrast, radars designed primarily for precision tracking may provide many more samples per resolution cell, allowing the use of different techniques.

The resolution of a radar system limits its ability to distinguish and accurately locate closely spaced targets, as described in Chapter 1. Figure 18-6 illustrates radar angular and range resolution. The two solid lines in the figure denote the one-way 3 dB beamwidth of the antenna, denoted here as θ_3. While the 3 dB points on the antenna gain pattern are often considered to define the angular *field of view* (FOV) of a radar system, the antenna gain pattern changes smoothly from the peak of the mainlobe to the first null and includes sidelobes at various angles from the antenna boresight. Although attenuated relative to echoes in the mainlobe, the energy of a sufficiently strong echo from a target or clutter outside the 3 dB points will often be observed in the output of the matched filter and can result in a detection threshold crossing. No specific angle in the antenna gain pattern other than a null ensures that target echo energy is not present in the output of the matched filter.

The dashed lines in Figure 18-6 partition the observation volume into *range gates*. This figure illustrates some of the problems that can occur when estimating range using a

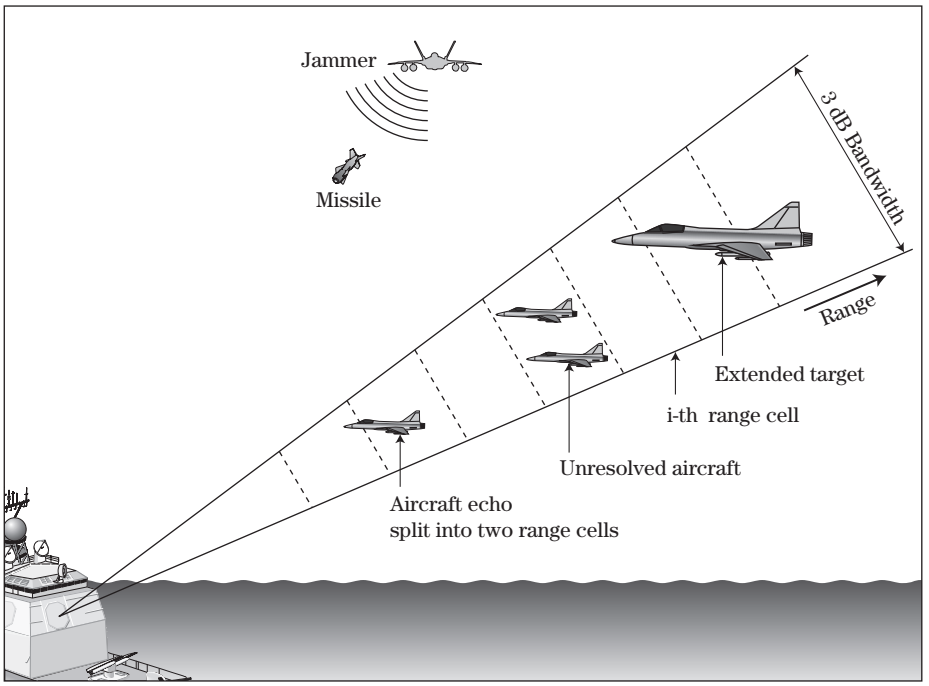

FIGURE 18-6 ■ Illustration of radar resolution with various targets. The solid lines show the two-way 3 dB beam pattern, while the dashed lines indicate range bins.

sampling interval equal to the range resolution. Each range cell is associated with a sample of the output of the matched filter through which the received echo signal is passed. The center of each range cell corresponds to the sample time. A range and angle measurement is made whenever the output of the matched filter exceeds the detection threshold. The small single aircraft is smaller than the extent of the range cell, but its position straddles two range cells, causing the echoed energy from the aircraft to be split between two adjacent range cells and incurring a straddle loss. Typically, every measurement experiences some straddle loss. The two closely spaced aircraft are in the same range cell, and only one measurement with energy from for both targets results. The large airliner extends over three range cells. Such targets are often referred to as *extended targets*. Significant echoes from the airliner are observed in three consecutive samples of the matched filter. Part of the challenge in radar tracking and data association is deciding whether a sequence of detections is one extended target or multiple closely spaced targets. Also, the signals from the jammer enter into the measurements of the missile between it and the radar and affect all of the range cells that are collected along the line of sight to the missile.

Continuing the discussion on range measurement, the various situations that can result are depicted in Figure 18-7, where the sequence of rectangles represent consecutive samples of the matched filter output and the fraction of the target energy captured in the sample is represented by the percentage fill of the rectangle. Some of these situations are analogous to those depicted in Figure 18-6. On the left side of the top sequence in Figure 18-7, the reflected energy is captured in a single sample of the matched filter output. However, this is typically not the case.

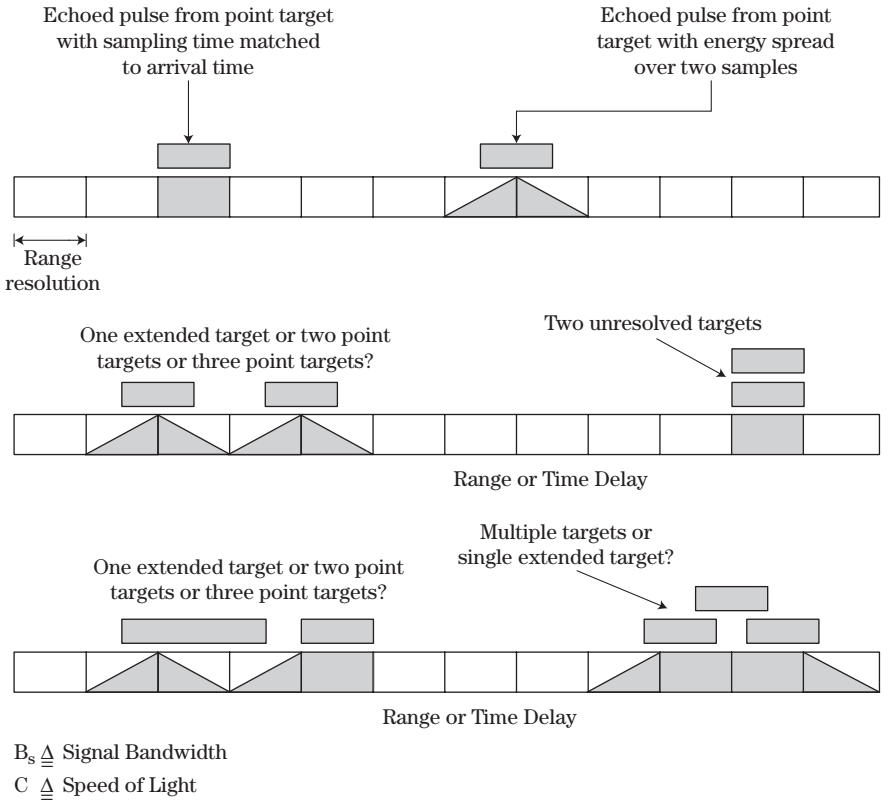

FIGURE 18-7 ■ Resolving closely spaced objects in range.

The more common case is illustrated by the sample of the echo in the top right of Figure 18-7, where the reflected energy is captured in two consecutive samples. In this case, the Cramèr-Rao lower bound on the variance of the range estimate is closely achieved by a power-weighted centroid of the ranges of the two consecutive samples. This technique, along with the split-gate centroid method of measuring range, are described and their precision analyzed in the next section. Examples of closely spaced single targets and multiple targets are shown in the other rows.

Sidelobes in range, angle, or Doppler complicate measurements further. Sidelobes are always present in angle due to the antenna sidelobes and in Doppler if the spectrum is computed using Fourier techniques, as will usually be the case. They will be present in range when pulse compression techniques are used. Sidelobes result in energy from the echo of a target being present in the data samples adjacent to those that correspond to the actual target location. For example, the echo of a small aircraft target with a relatively low RCS that is within a few of range cells of an airliner with a large RCS may be obscured by the range sidelobes from the airliner, a phenomenon known as *masking* (see Chapter 17 for an example of masking in the Doppler dimension). Waveform design methods and signal windowing techniques are often employed to reduce the impacts of range sidelobes. While special signal processing techniques can be employed to assist in the detection of unresolved or extended targets, multiple targets can appear as a single target measurement and one target can produce multiple measurements. Thus, close coordination of the signal processing and target tracking is needed.

18.5.2 Split-Gate and Centroid Range Measurement

In Sections 18.2.1 and 18.4.3 it was shown that target range measurement precision using the signal peak is dependent on the SNR. Rather than use the signal peak to estimate the range, a better approach is to use one of a number of techniques that combine multiple samples to provide some integration against noise. One such technique is an *early/late gate* or *split-gate* tracker. This technique is suitable for signals that produce outputs symmetric about the true location in the absence of noise. This is the case for both the angle and range measurement examples considered so far. The early/late gate tracker slides a two-part window across the data and integrates the energy within each of the two "gates" (halves of the window). When the energy in each gate is equal, the gate is approximately centered on the peak signal.

One way to implement the early/late gate tracker is to convolve the noisy output with the impulse response $h[l]$ shown in Figure 18-8b as the solid black line overlaid on the noisy data. The ideal (noise-free) matched filter output is shown in Figure 18-8a [see also Figure 18-2.] Because of the difference in sign of the impulse response in the two gates, the early/late gate tracker produces an output near zero when centered on the signal peak. This is depicted in Figure 18-9, which shows the magnitude of the output of the early/late gate tracker for input SNRs of 20 dB and 5 dB. The peak output of the matched filter (not shown) occurs at samples 99 and 107 in these two examples, while the early/late gate tracker correctly estimates the target range to be at sample 100 for the 20 dB case and misses by only 1 sample, at range bin 101, in the noisier 5 dB case. An alternative implementation does not take the magnitude at the tracker output; in this case, the range estimate is the zero crossing in the tracker output (see Chapter 19).

The precision of an early/late gate tracker is limited to the sampling density of the signal to which it is applied. This may be quite adequate if the data are highly oversampled

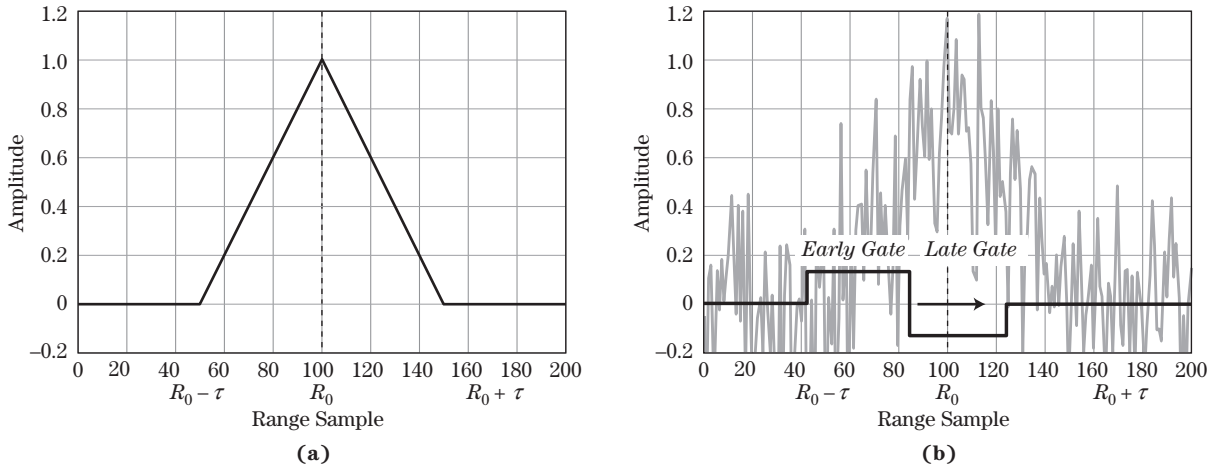

FIGURE 18-8 ■ (a) Triangular output of matched filter for an ideal rectangular pulse with no noise. (b) Output with 10 dB SNR. Also shown is an early/late gate tracker impulse response.

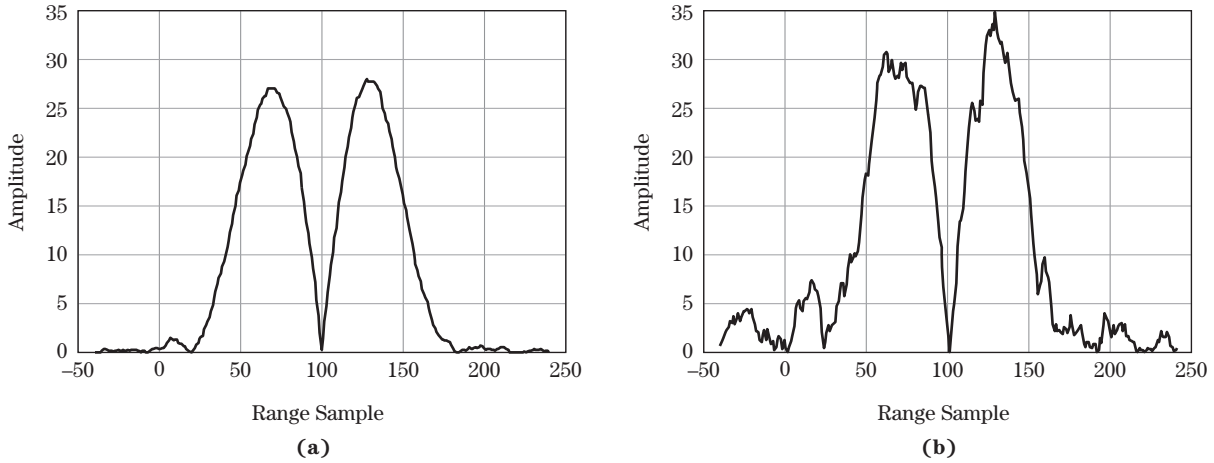

FIGURE 18-9 ■ (a) Magnitude of early/late gate tracker for simple pulse matched filter output with 20 dB peak SNR. (b) Output with 5 dB peak SNR.

(many samples per resolution cell), but, as discussed earlier, range is often estimated using data sampled at intervals approximately equal to a resolution cell. An alternative to the early/late gate tracker is the *centroid* tracker. The centroid, C_x, over a region $l \in [L_1, L_2]$ of a sequence $x[l]$ is defined as

$$C_x = \frac{\sum_{l=L_1}^{L_2} l \cdot x[l]}{\sum_{l=L_1}^{L_2} x[l]} \tag{18.35}$$

Note that the centroid can take on a noninteger value, so it inherently interpolates between samples.

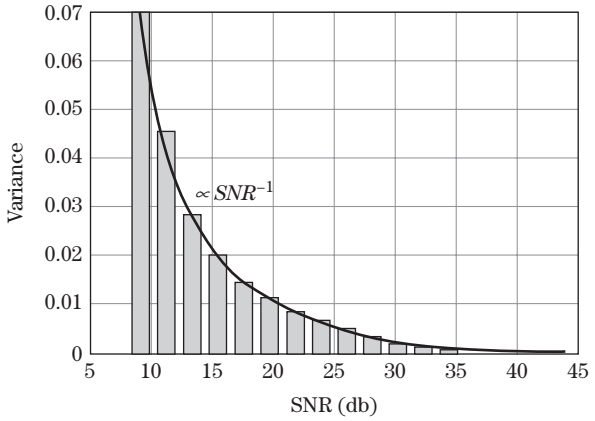

FIGURE 18-10 ■ Example of variance of power-weighted centroid range estimation for ideal simple pulse and matched filter. The variance is normalized to the range resolution.

To demonstrate the performance of the two-point power centroid, consider an ideal rectangular pulse of duration τ and a matched filter. The output of the matched filter is a triangular pulse of duration 2τ (Chapter 20; see also Figure 18-2). A square law detector is assumed. The magnitude squared of the filter output is sampled at the nominal range resolution (i.e., every τ seconds). A two-point power centroid is applied and the range estimation error is calculated after removing the bias of the estimator for the noise-free case. The error depends on the location of the actual target peak relative to the sampling times, so it is averaged over sampling times that vary by $\pm\tau/2$ seconds relative to the peak. The resulting variance of the average estimation error, normalized to the range resolution, is shown in Figure 18-10 as a function of SNR. The error variance decreases approximately as $1/SNR$ for the range of SNR shown.

An approximation to the CRLB of the range measurement for a simple, uncoded, rectangular pulse is given in [6] as

$$\sigma_R^2 \geq \frac{c^2\tau}{8SNR \cdot B_{IF}} \tag{18.36}$$

where B_{IF} is the bandwidth of the IF filter, and τ is the pulse duration. A power-weighted centroid of the ranges of the two consecutive samples approaches this CRLB. More detail on measurement precision for closely spaced targets is given in [6]. Resolving two closely spaced targets in range is addressed in [7,8]. When range is measured with a linear frequency modulated (LFM) waveform, any uncompensated Doppler shift results in a shift in the apparent range of the target, a phenomenon called range-Doppler coupling (see Chapter 20). The CRLB for range measurement using an LFM waveform with a rectangular envelope and a known range rate is given in [9] as

$$\sigma_R^2 \geq J(R) = \frac{3c^2}{8\pi^2 SNR \cdot B^2} \tag{18.37}$$

where B is the swept bandwidth of the LFM waveform.

18.6 PHASE MEASUREMENT

Estimating the echo time of arrival using the methods previously described ignores the signal phase. However, signal phase can also be estimated if the Doppler shift is known. Combining terms to simplify the signal model in equation (18.1) when the frequency is

known, the radar return can be written as

$$s(t) = p(t)\cos(\omega t + \varphi) \tag{18.38}$$

where ω is the frequency, and φ is the carrier phase. It can then be shown that the optimal estimator for the phase is [4]

$$\hat{\varphi} = -\tan^{-1}\frac{P_s}{P_c} \tag{18.39}$$
$$P_s = \int p(t)\sin(\omega t)dt \qquad P_c = \int p(t)\cos(\omega t)dt$$

where the sine and cosine filter integrals are over the analysis time window. When the SNR is sufficiently large the RMS error is [4]

$$\sigma_{\hat{\varphi}}^2 \geq \frac{1}{SNR \cdot \tau B} \tag{18.40}$$

where τB is the pulse time-bandwidth product. Note that, like range estimation, the phase measurement variance is inversely proportional to the measurement SNR.

18.7 | DOPPLER AND RANGE RATE MEASUREMENTS

In most modern tracking radars, range rate measurements are accomplished by pulsed Doppler waveforms that include a periodic sequence of pulses. In pulse-Doppler processing, the output of the matched filter is sampled throughout the range window for each pulse for time-delay (i.e., range) estimation, and samples of the matched-filter output from the multiple pulses at each range are processed with a DFT to estimate the Doppler frequency, f_d (also known as range rate, $\dot{R}$). The Doppler resolution is the inverse of the duration of the pulse-Doppler waveform dwell time, T_d (see Chapter 14),

$$\Delta f_d = \frac{1}{T_d} \tag{18.41}$$

Because velocity is related to Doppler shift according to $f_d = 2v/\lambda$, the resolution of velocity or range rate is

$$\Delta v = \Delta\dot{R} = \frac{c}{2T_d f_t} = \frac{\lambda}{2T_d} \tag{18.42}$$

where f_t is the carrier frequency of the transmitted waveform.

Pulse-Doppler waveforms suffer potential *ambiguities* in range and range rate. The minimum unambiguous range is

$$R_{ua} = \frac{c}{2}PRI \tag{18.43}$$

For a slow-time sampling interval (PRI) of T seconds, the ambiguous interval in Doppler frequency is $1/T$ Hz. Assuming both positive and negative frequencies (and thus range rates) are of interest, the maximum unambiguous Doppler frequency, velocity, and range

rate are then given by

$$f_{d_{ua}} = \pm\frac{1}{2PRI} = \pm\frac{PRF}{2}$$
$$v_{ua} = \dot{R}_{ua} = \pm\frac{\lambda}{2}PRF = \pm\frac{c}{2f_t}PRF \tag{18.44}$$

Thus, the range rate resolution is specified by the dwell time of the waveform, while the maximum unambiguous range rate is specified by the PRF of the waveform.

The CRLB for measuring frequency in hertz for the signal model of equation (18.2) with M measurements, assuming the initial phase and amplitude are also unknown, is shown by several authors to be [3,4]

$$\sigma_f^2 \geq J(f) = \frac{3f_s^2}{\pi^2 SNR \cdot M(M^2-1)} \approx \frac{3f_s^2}{\pi^2 SNR \cdot M^3} \quad \text{Hz}^2 \tag{18.45}$$

where f_s is the sampling frequency in samples/second. Notice that the CRLB decreases as M^3. One factor of M comes from the increase in SNR when integrating multiple pulses, while a factor of M^2 comes from the improved resolution of the frequency estimate. This can be seen by putting equation (18.45) into terms of resolution and SNR for the case of an estimator based on the discrete-time Fourier transform (DTFT), of which the DFT is a special case. The Rayleigh frequency resolution in hertz of an M-point DFT is f_s/M, and the SNR of a sinusoidal signal in the frequency domain is M times the time-domain SNR, assuming white noise (see Chapter 14). Denoting the frequency domain resolution and SNR as Δf and SNR_f, equation (18.45) becomes

$$\sigma_f \geq \frac{\sqrt{3}}{\pi}\frac{\Delta f}{\sqrt{SNR_f}} \quad \text{Hz} \tag{18.46}$$

Equation (18.46) states that the precision of the frequency estimate is proportional to the resolution divided by the square root of the applicable SNR, analogous to the range estimation case of equation (18.33).

A number of single and multi-pulse frequency estimation schemes exist. These can be divided into coherent and noncoherent techniques [4]. Several are considered in the following. Other general frequency estimation techniques are considered in [3].

18.7.1 DFT Methods

An obvious estimator of Doppler frequency is the discrete Fourier transform, usually implemented with the fast Fourier transform (FFT) algorithm. Given M samples of slow time data $y[m]$, the K-point DFT is

$$Y[k] = \sum_{m=0}^{M-1} y[m]\exp\left[-j2\pi mk/K\right], \quad k = 0, \ldots, K-1 \tag{18.47}$$

where $K \geq M$. The DFT and its properties are discussed extensively in Chapter 14.

The frequency of a signal is estimated by computing its DFT and then finding the value of k that gives the largest value of $Y[k]$, that is, by finding the peak of the DFT. The k-th index corresponds to a frequency of $k{\cdot}PRF/K$ Hz. Consider a signal

$$y[m] = A\exp\left[j2\pi f_0 mT\right] + w[m], \quad m = 0, \ldots, M-1 \tag{18.48}$$

where $w[m]$ is white Gaussian noise with power σ_w^2. The SNR of the individual data samples is A^2/σ_w^2. The DFT effectively integrates the M data samples, increasing the SNR to a maximum of MA^2/σ_w^2 if f_0 equals one of the DFT frequencies. If f_0 does not equal one of these frequencies, the integrated SNR is up to 3.92 dB lower (depending on the frequency difference and the data window used; see Chapter 14 for details). This reduction is another example of straddle loss.

If the integrated SNR is at least 10 dB, it is virtually certain that the DFT peak will occur at the index closest to the true frequency as desired. Then, for a sinusoidal signal at an arbitrary frequency f_0, the maximum error in the estimated frequency $\hat{f}_0$ is $PRF/2K$ Hz. Thus, increasing the DFT size reduces the maximum frequency estimation error, at the cost of increased computational load for the larger DFT. The same CRLB for frequency estimation given by equation (18.45) applies [3].

18.7.2 DFT Interpolation Methods

Frequency estimation precision can be improved following the DFT calculation with one of a number of interpolation methods. The centroiding technique discussed earlier for range processing can be applied to the DFT also. Another common method is to fit a low-order polynomial through the DFT peak and its nearest neighbors. The estimated frequency is the location of the peak of the interpolated polynomial. A typical interpolator, using only the magnitude of the DFT samples, estimates the frequency as [10]

$$\begin{aligned} \Delta k &= \frac{-\frac{1}{2}\{|Y[k_0+1]| - |Y[k_0-1]|\}}{|Y[k_0-1]| - 2|Y[k_0]| + |Y[k_0+1]|} \\ \hat{f}_0 &= \frac{(k_0+\Delta k)}{K} PRF \end{aligned} \tag{18.49}$$

where k_0 is the index at which the DFT peak occurs. Figure 18-11a shows the precision of this estimate, $f_0 - \hat{f}_0$, as a function of the starting offset $f_0 - k_0 PRF/K$ for $M = 30$ data samples and various DFT sizes K. Note that the precision improves as the DFT size increases.

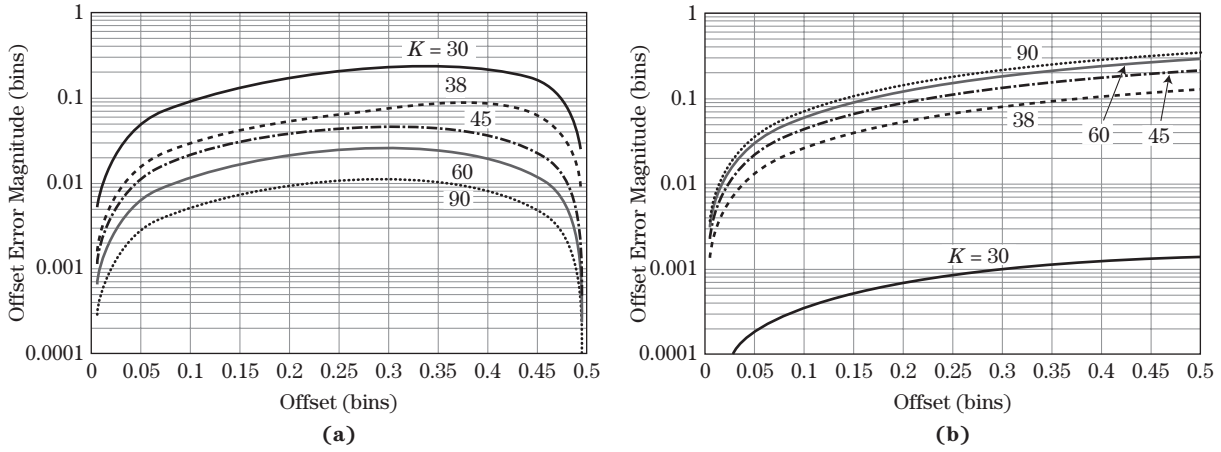

FIGURE 18-11 ■ Precision of DFT interpolators. Data length $M = 30$. (a) Magnitude only. (b) Magnitude and phase.

Figure 18-11b shows the precision of a similar interpolator that uses the complex DFT data instead of just the magnitude. The estimate is given by [10]

$$\Delta k = -\mathrm{Re}\left\{ \frac{Y[k_0+1] - Y[k_0-1]}{2Y[k_0] - Y[k_0-1] - Y[k_0+1]} \right\}$$
$$\hat{f}_0 = \frac{(k_0 + \Delta k)}{K} PRF \tag{18.50}$$

This estimator achieves much better precision than the estimator of equation (18.49) when $K = M$, but the precision actually gets worse as K gets larger! Another complication with these interpolators is that they must be modified if a window is used on the data, and the modification required depends on the specific window being used. Examples and additional details are given in [10].

18.7.3 Pulse Pair Estimation

Pulse pair processing (PPP) is a specialized form of Doppler measurement common in meteorological radar. In PPP, it is assumed that the spectrum of the slow-time data consists of noise and a single Doppler peak, generally not located at zero Doppler (though it could be). The goal of PPP is to estimate the power, mean velocity, and *spectral width* (variance) of this peak. PPP is used extensively in both ground-based and airborne weather radars for storm tracking and weather forecasting. In airborne radars, it is also used for windshear detection. Additional detail is available in [1,11].

The notional frequency spectrum, $S_y(f)$, assumed by PPP is shown in Figure 18-12. It consists only of white noise and a single spectral peak:

$$S_y(f) = S_s(f) + P_w \tag{18.51}$$

The spectral peak of the signal component, $S_s(f)$, is usually assumed to be approximately Gaussian shaped and is characterized by its amplitude, mean, and standard deviation. Under this assumption, $S_s(f)$, will be of the form

$$S_s(f) = \frac{P_s}{\sqrt{2\pi}\sigma_f} e^{-(f-f_0)^2/2\sigma_f^2} \tag{18.52}$$

If the slow-time sampling interval, T, is chosen sufficiently small to guarantee that $S_{s'}(1/2T) \approx 0$, then it can be shown that the discrete time autocorrelation function is

$$s_y[k] = P_s e^{-2\pi^2\sigma_f^2 k^2 T^2} e^{-j2\pi f_0 kT} + P_w \cdot \delta[k] \tag{18.53}$$

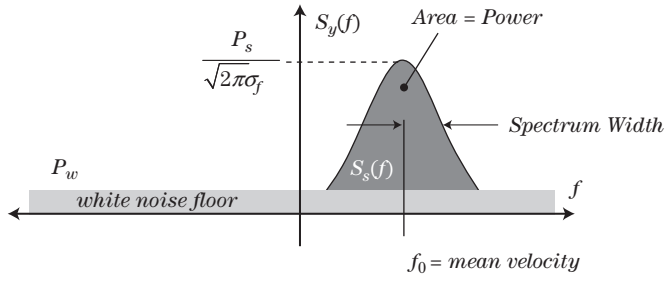

FIGURE 18-12 ■ Power spectrum model for pulse pair processing.

Pulse pair processing is a simple algorithm for estimating the parameters P_s, f_0, and σ_f using only two computed autocorrelation values of the slow-time data for a given range bin. The estimation equations are derived in [1,11]; only the results are given here. Define the deterministic autocorrelation of the slow-time data sequence $y[m]$, $m = 0, \ldots, M-1$ as

$$s_y[k] \equiv \sum_{m=0}^{M-k-1} y[m]\ y^*[m+k] \tag{18.54}$$

From equation (18.53), $s_y[0] = P_s + P_w$. Combining this with equation (18.54) gives

$$P_y = P_s + P_w = s_y[0] = \sum_{m=0}^{M-1} |y[m]|^2 \tag{18.55}$$

If an estimate $\hat{P}_w$ of the noise power is available, the signal power can be estimated as

$$\hat{P}_s = \hat{P}_y - \hat{P}_w \tag{18.56}$$

A noise power estimate can usually be obtained by averaging spectral samples near $\pm\, PRF/2$, possibly over a number of range bins.

The mean frequency of the spectral peak can be estimated as

$$\hat{f}_0 = \frac{-1}{2\pi T} \arg\{s_y[1]\} \tag{18.57}$$

This estimator works well provided there is a single dominant frequency component with adequate signal-to-noise ratio. Note that the frequency estimate is aliased if the actual frequency exceeds $PRF/2$.

Finally, it is easy to verify from the previous equations that the spectral width can be estimated as

$$\hat{\sigma}_f^2 = -\frac{1}{2\pi^2 T^2} \ln\left\{\frac{|s_y[1]|}{s_y[0] - \hat{P}_w}\right\} = -\frac{1}{2\pi^2 T^2} \ln\left\{\frac{|s_y[1]|}{\hat{P}_s}\right\} \tag{18.58}$$

Equations (18.55), (18.57), and (18.58) are the time-domain pulse pair processing estimators. They can be computed from only two autocorrelation lags of the slow-time data.

The basic PPP measurements of signal power, frequency, and spectral width can also be performed in the frequency domain. These methods are discussed in more detail in [11]. Generally, the time-domain estimators are preferred if the signal-to-noise ratio is low or the spectral width is very narrow. In addition, the time-domain methods are more computationally efficient, because no Fourier transform calculations are required.

18.8 RCS ESTIMATION

The radar cross section, σ, of a target is related to the target echo signal amplitude, ξ, through the radar range equation as shown in equation (18.6). The actual amplitude available for measurement is Λ of equation (18.7). Consider the measured power $P_s = \Lambda^2$ of the complex signal $s = s_I + js_Q$. P_s is the combination of the target echo power and the noise power and thus is a random variable. The expected value of P_s is

$$\overline{P}_s = \alpha^2 + \sigma_w^2 \tag{18.59}$$

If $\overline{P}_s$ can be estimated and an estimate of the noise power σ_w^2 is available, then equation (18.59) can be used to estimate α^2, which can be used in turn with the radar range equation and equation (18.3) to estimate the amplitude reflectivity, ξ, and the RCS, σ. In this section procedures for estimating $\overline{P}_s$ from M samples are considered.

The optimal estimator for the power depends on its PDF. Recall from Chapter 15 that various fluctuation models are used to model target echoes and that the nonfluctuating and Swerling models are among the most common. However, a simple suboptimal estimator usable with any PDF is the sample mean,

$$\widehat{\overline{P}_s} = \frac{1}{M}\sum_{m=0}^{M-1} P_s[m] \tag{18.60}$$

where $P_s[m]$ denotes the m-th sample of the measured power, typically the power measured on the m-th pulse of an M-pulse dwell. The CRLB for this case was given by equation (18.23).

Now consider the Swerling 2 target. In this case, the RCS is exponentially distributed and is uncorrelated pulse to pulse. The resulting measured power is also exponentially distributed (see Chapter 15 or [1]). Specifically,

$$p_{P_s}(P_s) = \frac{1}{\overline{P}_s}\exp\left(-P_s/\overline{P}_s\right) \tag{18.61}$$

where $\overline{P}_s$ is the expected value of the received power. Note that this PDF is fully specified by the single parameter, $\overline{P}_s$. It is easy to show that the maximum likelihood estimator of the parameter $\overline{P}_s$ is simply the sample mean, that is, equation (18.60) [1,12]. Consequently, the sample mean is an optimal estimator for this case. Problem 4 at the end of this chapter derives the CRLB for this case.

In the Swerling 4 and nonfluctuating cases, the PDF of P_s is significantly more complicated, and simple analytical expressions for the ML estimator do not exist. The CRLB also does not have a closed form. For some cases, it can be shown that for moderate to high SNRs, the ML estimator is approximately equal to the sample mean of equation (18.60) [12]. Thus in practice, the sample mean is usually used to estimate P_s for most common target models.

18.9 ANGLE MEASUREMENTS

A target echo that is received through a standard antenna pattern gives no information about the angular location of the target other than it is most likely within the mainlobe of the beam as noted earlier. If a target has a large RCS, it may not even be within the 3 dB beamwidth of the antenna pattern. In most radars that rotate for scanning the field of regard, the amplitudes of the echoed signals are collected for multiple positions of the antenna boresight as it scans by the target, and centroiding is used to estimate the angular location of the target. However, for tracking radars that support control functions, radars that measure two angular coordinates, and electronically scanned radars that scan while tracking, centroiding the signals from multiple positions of the antenna pattern is not a viable option because many beam positions are needed to overcome the RCS fluctuations of the target for an accurate angle-of-arrival estimate.

One of the techniques used early on to improve the angle measurements of this type of radars was *sequential lobing*, which uses two consecutive dwells on the target to refine

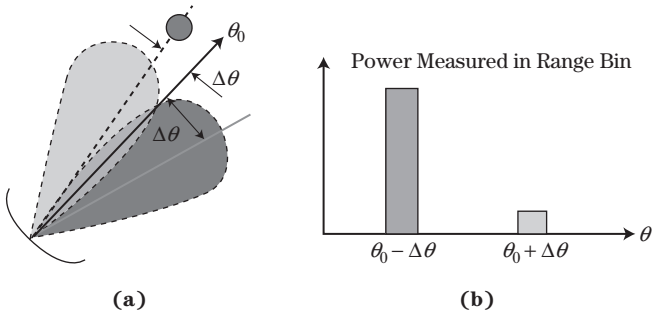

FIGURE 18-13 ■ Notional illustration of sequential lobing for direction determination. In (a) the target is observed first at one angle, then at a second. Due to the antenna gain pattern the differences in observation angle result in different return powers as illustrated in (b).

each angle measurement [13]. As illustrated in Figure 18-13, the first measurement is taken with the boresight of the antenna pointing slightly to one side of the predicted target position, while the second measurement is taken with the boresight of the antenna pointing slightly to the other side of the predicted position. Then the target is declared to be closer to the angle of the measurement with the larger amplitude, and the predicted angle of the target is corrected. However, sequential lobing is very susceptible to pulse-to-pulse amplitude fluctuations of the target echoes, which are common in radar measurements due to scintillation in the RCS of the target. Furthermore, when tracking in azimuth and elevation, sequential lobing requires lobe switching between azimuth and elevation or conical scanning (see Figure 18-14) [13], both of which are inefficient with respect to radar time and energy and are easily jammed or deceived by the intended target.

Monopulse is a simultaneous lobing technique that was developed to overcome the shortcomings of sequential lobing and conical scanning [13]. Monopulse antennas were described in Chapter 9. In an *amplitude comparison monopulse* radar system, a pulse is transmitted directly at the predicted position of the target, and the target echo is received with two squinted beams ("split beams"). Figures 18-15 and 18-16 illustrate the transmit and difference antenna patterns for a single-dimensional monopulse. The angle of arrival of the target is typically estimated with the in-phase part (i.e., the real part) of the monopulse ratio, which is formed by dividing the difference of the two received signals by their sum (see Figure 18-16). When tracking in azimuth and elevation, four beams are used for receive, and two monopulse ratios are typically formed. The simultaneous lobing of

FIGURE 18-14 ■ Conical sequential lobing illustration.

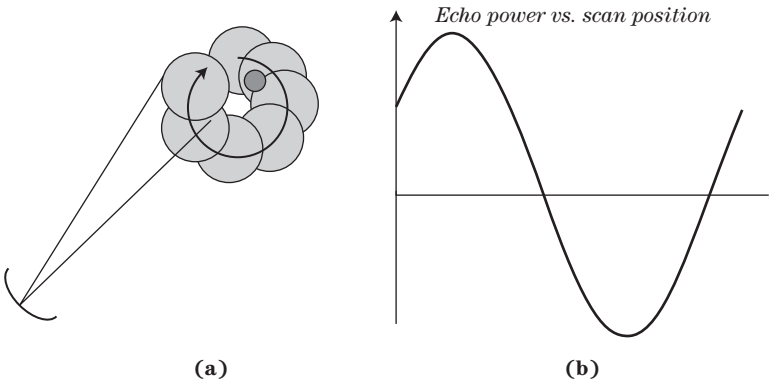

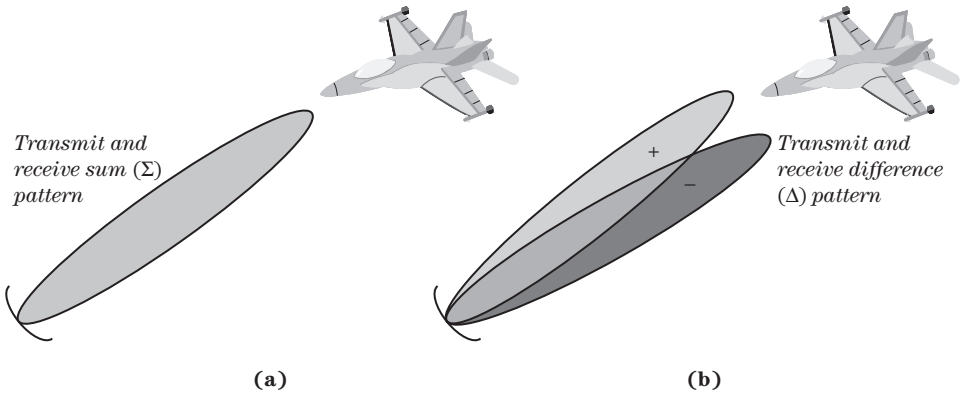

FIGURE 18-15 ■ Notional antenna patterns for a monopulse angle-of-arrival system. (a) Sum channel. (b) Difference pattern.

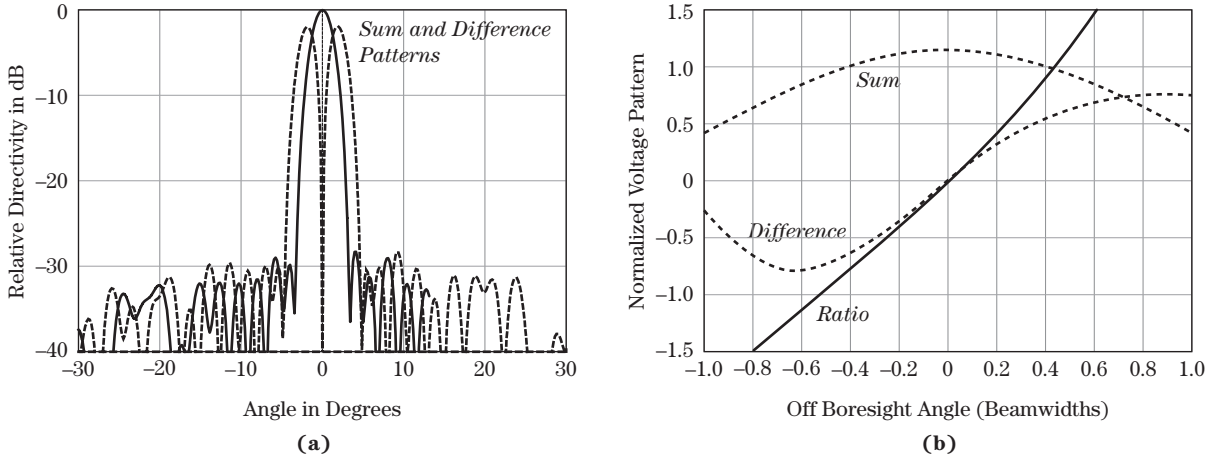

FIGURE 18-16 ■ Monopulse antenna gain patterns. (a) Solid line is the sum channel gain while dotted line is the difference channel gain. (b) Plots of the sum and difference channel gains and their ratio near the boresight.

monopulse allows the transmitted energy to be directed at the predicted position of the target and eliminates the errors due to amplitude fluctuations by forming a refinement of the angular precision with a single pulse.[1] Since the lobing is simultaneous rather than sequential, monopulse is very efficient with respect to radar time and energy and difficult to jam or deceive. Both of these benefits are particularly important to electronically steered radars that are required to maintain simultaneous tracks on many targets.

An alternative approach to amplitude comparison monopulse is *phase comparison monopulse* [4]. Phase comparison monopulse is a form of radar interferometry that relies on phase differences between the antenna beams, often achieved by offsetting two antennas, to determine the angle to the target. As illustrated in Figure 18-17 a baseline between the

[1]The term *monopulse* originated with this idea of a single-pulse refinement of the angular accuracy. Some confusion exists concerning monopulse radars because many monopulse radars use multiple pulses to form an angular measurement. The monopulse ratios formed with each pulse are what distinguishes a radar as monopulse.

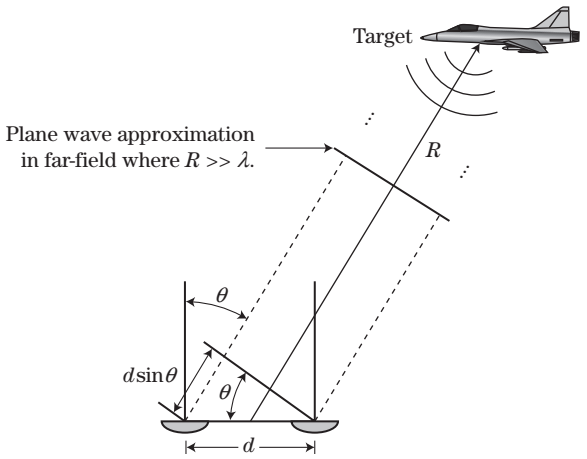

FIGURE 18-17 ■ Geometry of phase comparison monopulse. The displacement distance *d* between the antennas causes different path lengths to the target, which gives rise to a difference in phase of the return echo between the two beams. The target is assumed to be far enough away that the far-field approximation applies.

two beam phase centers creates a path length difference, $d\sin\theta$, to the target, which results in a phase difference in the signals. An important practical limitation in AOA measurement using phase comparison monopulse is that, to prevent ambiguity in the estimated direction, the target angle and antenna baseline separation must meet the requirement [13]

$$|\sin\theta| < \frac{\lambda}{8d} \tag{18.62}$$

Both monopulse and centroiding are used for AOA estimation in modern radar systems. Implementing a monopulse AOA system is more expensive than implementing a centroiding AOA system. However, the time occupancy requirements of electronically scanned radars for multiple target tracking dictate the use of monopulse AOA estimation. In the remainder of this section, centroiding and monopulse AOA estimation are discussed.

18.9.1 Angle Centroiding for Scanning Radars

When considering the AOA estimation method for a rotating radar, centroiding should be the first consideration. The estimation error of an angle centroider depends on the single-pulse SNR, the number of pulses transmitted within the antenna beamwidth, the antenna gain pattern, and target fluctuation model. Two basic approaches to AOA centroiding are the *binary integration* approach [14] and the ML approach [15]. The binary integration approach is motivated by the need to limit memory and processing in real-time radar systems, while the ML approach is motivated by the need for more accurate estimation. However, studies have found that the AOA estimation of binary integration can approach the CRLB for sufficiently high SNR and targets with rather stable radar cross sections. For Swerling targets, the CRLB for the AOA has the following form [14,16]

$$\sigma_\theta^2 = \frac{\theta_3^2}{N \cdot SNR \cdot \alpha^2} \tag{18.63}$$

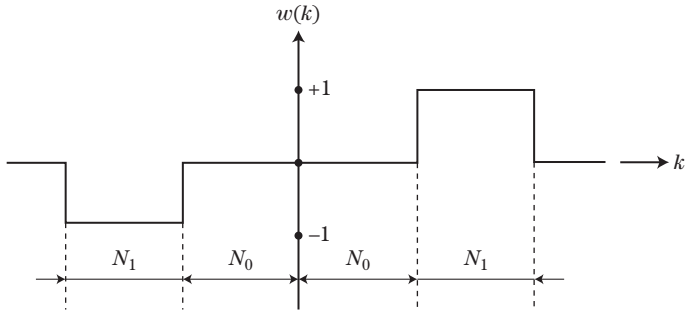

FIGURE 18-18 ■ Weights of a binary Bernstein estimator for angle-of-arrival centroiding.

where θ is the AOA, θ_3 is the 3 dB beamwidth of the antenna pattern, N is the number of pulses in the azimuth interval, and α is a constant that depends on the ratio of the azimuth observational interval and the 3 dB antenna beamwidth. For a large azimuth observation interval, $\alpha \approx 0.339$. While the performance of a centroider depends on many parameters, an AOA centroider can be expected to achieve $\sigma_\theta \approx \theta_3/10$, where σ_θ is the standard deviation of the error in the AOA estimate.

In the binary integration approach, the samples of the matched filter output are quantized to 0 or 1. For a given scan of the radar by the target, an AOA estimate can be produced by taking a simple average of the angle of the antenna boresight at the first detection of the target (i.e., the leading edge) and the angle of the antenna boresight at the final detection of the target (i.e., the trailing edge). For targets with very stable echoes, this simple approach performs reasonably well. However, for targets with fluctuating amplitudes, a better method is needed. An improved approach is represented by the Bernstein estimator [14] in which the quantized detections are convolved with the weights shown in Figure 18-18. The Bernstein estimator uses N_1 detection opportunities that occur as the antenna boresight scans toward the target and N_1 detection opportunities that occur as the antenna boresight scans away from the target to reduce the sensitivity of the AOA estimate to amplitude fluctuations. The convolution of those detection opportunities with the Bernstein weights gives rise to a zero crossing that corresponds to the AOA estimate of the target. The $2N_0 - 1$ detection opportunities that occur when the antenna boresight is closely aligned with the target are ignored by the Bernstein estimator as those samples provide very little or no information concerning the AOA of the target. Typically, $2(N_0 + N_1) \approx N$. Optimal values for N_0 and N_1 are a function of the SNR of the target and the fluctuation model. Thus, the diversity of targets with respect to RCS and fluctuations make it impossible to achieve optimal AOA estimation without adaptation.

The ML approach to centroiding for AOA estimation involves formulating the measured amplitude of the target echoes in terms of the antenna gain pattern and the angle of the target and computing the ML estimate of the target AOA. The target amplitude is typically treated as a fixed, unknown quantity over the scan, which is a reasonable assumption for many targets if the pulses include at least 10 MHz of frequency agility.

18.9.2 Monopulse AOA Estimation

While most monopulse systems include AOA estimation to two angular coordinates, only monopulse processing in a single angular coordinate is considered in this section. The focus is on amplitude-comparison monopulse. Only the monopulse processing for Rayleigh targets is considered here. The monopulse signals are formulated, and conventional monopulse processing is discussed first.

18.9.2.1 Single Target

Using the notation in Section 18.3, equation (18.2) gives the sum signal for the monopulse processing, while the vertical difference signal is given by

$$d(t) = 2\sqrt{\frac{P_t}{(4\pi)^3}}\frac{G_t\lambda}{R^2}AG_\Sigma(\theta,\psi)G_{\Delta V}(\theta,\psi)p(t)\cos(\omega_c t + \omega_d t + \phi) + w_d(t) \quad (18.64)$$

where $G_\Sigma(\theta,\psi)$ denotes the voltage gain of the antenna in the sum channel at (θ,ψ), $G_{\Delta V}(\theta,\psi)$ denotes the voltage gain of the antenna in the vertical difference channel at (θ,ψ), (θ,ψ) denotes the angular location of the target relative to antenna boresight, and $w_d(t)$ denotes the receiver noise in the vertical difference channel. A similar difference signal will also be received for the horizontal coordinate. Note that "vertical" and "horizontal" are used to denote the two orthogonal coordinates of the radar. These differ from the local horizontal and vertical if the antenna boresight is tilted out of the horizontal plane.

Monopulse is implemented slightly differently in phased array radars. In a phased array radar, two beamforming networks (three networks for monopulse in two angles) are used to simultaneously form sum and difference beams. The sum pattern as given in Section 18.3 may be used for transmit and receive in the sum channel, while the difference pattern may be the result of subtracting two beams, each formed with one-half of the array. Ignoring the Doppler and straddle losses, the in-phase and quadrature components of the sum (s_I and s_Q) signal and difference (d_I and d_Q) signal are given by

$$\begin{array}{ll} s_I = \alpha\cos\phi + w_{sI} & s_Q = \alpha\sin\phi + w_{sQ} \\ d_I = \alpha\eta\cos\phi + w_{dI} & d_Q = \alpha\eta\sin\phi + w_{dQ} \end{array} \quad (18.65)$$

where κ is a constant that depends on the target amplitude, system gain, and transmit power and

$$\alpha = \kappa G_\Sigma(\theta,\psi), \quad \eta = \frac{G_{\Delta V}(\theta,\psi)}{G_\Sigma(\theta,\psi)}, \quad (18.66)$$

$$w_{sI} \sim N\left(0,\sigma_s^2\right), \quad w_{sI} \sim N\left(0,\sigma_s^2\right), \quad w_{dI} \sim N\left(0,\sigma_d^2\right), \quad w_{dQ} \sim N\left(0,\sigma_d^2\right)$$

The receiver errors in the sum and difference channels are typically uncorrelated except for a possible real-valued correlation or $E(n_{sI}n_{dI}) = E(n_{sQ}n_{dQ}) = \rho\sigma_d\sigma_s$ [13]. Since the parameter η defines an off-boresight angle θ, η is referred to as the AOA parameter. Thus, monopulse processing involves the estimation of η and using the estimate of η to compute the AOA relative to the antenna boresight.

In a typical monopulse system, the AOA with respect to the antenna boresight is approximated by

$$\theta \approx \frac{\theta_3}{k_m}\eta \quad (18.67)$$

where $1 < k_m < 2$ and θ_3 is the 3 dB beamwidth of the antenna pattern. The linear approximation to the monopulse error function is usually appropriate for $-\theta_3/2 \le \theta \le \theta_3/2$. Denoting $s = s_I + js_Q$ and $d = d_I + jd_Q$, the in-phase and quadrature parts of the monopulse ratio are given by

$$y_I = \mathrm{Re}\left(\frac{d}{s}\right) = \frac{d_I s_I + s_Q d_Q}{s_I^2 + s_Q^2}, \quad y_Q = \mathrm{Im}\left(\frac{d}{s}\right) = \frac{d_Q s_I - d_I s_Q}{s_I^2 + s_Q^2} \quad (18.68)$$

Typically, y_I is taken as the estimate of the direction on arrival (DOA), which gives the AOA estimate as

$$\hat{\theta} = \frac{\theta_3}{k_m}\left(y_I - \rho\frac{\sigma_d}{\sigma_s}\right) \tag{18.69}$$

The variance of y_I is often reported in the literature [13] as

$$\sigma_{y_I}^2 \approx \frac{1}{2 \cdot SNR}\left[\frac{\sigma_d^2}{\sigma_s^2} + \eta^2 - 2\rho\frac{\sigma_d}{\sigma_s}\right], \quad SNR > 13 \text{ dB} \tag{18.70}$$

where SNR is the signal-to-noise of the sum channel signal. Estimates of the variance of y_I are often computed by setting $\eta = y_I$. An estimate of the variance of the AOA is then given by

$$\sigma_{\hat{\theta}}^2 \approx \frac{\theta_3^2}{k_m^2}\sigma_{y_I}^2 \approx \frac{\theta_3^2}{2k_m^2 SNR}\left[\frac{\sigma_d^2}{\sigma_s^2} + y_I^2 - 2\rho\frac{\sigma_d}{\sigma_s}\right], \quad SNR > 13 \text{ dB} \tag{18.71}$$

Several authors have shown that y_I is a notably biased[2] estimate of the DOA at moderate and low SNR. The bias is often reported in the literature [13] as

$$E(y_I) - \eta = \left(\rho\frac{\sigma_d}{\sigma_s} - \eta\right)\exp(-SNR) \tag{18.72}$$

Seifer showed in [17] that this is an optimistic assessment of the bias because the measured amplitude of the sum signal is subjected to a threshold test prior to monopulse processing.

For a Rayleigh target with real uncorrelated receiver errors, the joint PDF of the in-phase and quadrature parts of the monopulse ratio is given by

$$p_{y_I,y_Q}\left(y_I, y_Q \middle| SNR_{\text{obs}}\right) = p_{y_I}\left(y_I \middle| SNR_{\text{obs}}\right) p_{y_Q}\left(y_Q \middle| SNR_0\right) \tag{18.73}$$

where SNR_{obs} is the observed SNR $\alpha^2\eta^2/\sigma_d^2$ and

$$\begin{aligned} p_{y_I}(y_I|SNR_{\text{obs}}) &= \text{N}\left(\frac{SNR \cdot \eta + \rho\sigma_d\sigma_s^{-1}}{SNR+1}, \frac{\gamma}{2SNR_{\text{obs}}}\right) \\ p_{y_Q}(y_Q|SNR_{\text{obs}}) &= \text{N}\left(0, \frac{\gamma}{2SNR_{\text{obs}}}\right) \\ \gamma &= \left[\frac{\sigma_d^2}{\sigma_s^2}\left(1 - \frac{\rho^2}{SNR+1}\right) + \frac{SNR \cdot \eta\left(\eta - 2\rho\sigma_d\sigma_s^{-1}\right)}{SNR+1}\right] \end{aligned} \tag{18.74}$$

The notation $\text{N}(\mu, \sigma^2)$ denotes a normal (Gaussian) distribution with mean μ and variance σ^2. Thus, y_I and y_Q are conditionally Gaussian, independent random variables. Note that equation (18.74) shows that even for $\rho = 0$, y_I is a notably biased observation of the DOA η for values of SNR less than about 13 dB.

[2] *Notably biased estimate* is used here to denote an estimate with bias greater than 5% of the true value.

Let $\bar{y}_I$ denote the mean of y_I given SNR_{obs}. Then, for N independent samples or pulses, the ML estimate of $\bar{y}_I$ is given by

$$\hat{y}_I = \frac{1}{NY_N}\sum_{k=1}^{N} SNR_{\text{obs}_k} y_{I_k}, \qquad Y_N = \frac{1}{N}\sum_{k=1}^{N} SNR_{\text{obs}_k} \tag{18.75}$$

where SNR_{obs_k} and y_{I_k} denote the observed SNR and in-phase monopulse ratio for pulse k, respectively. Thus, the estimate $\hat{y}_I$ is a "power" or "energy" weighted sum of the N monopulse ratios. Since the y_{Ik} are Gaussian random variables, $\hat{y}_I$ is the minimum variance estimate of $\bar{y}_I$ and a Gaussian random variable with variance given by

$$\sigma^2_{\hat{y}_I} = \frac{\gamma}{2NY_N} \tag{18.76}$$

where γ was defined in equation (18.74). However, note that $\hat{y}_I$ being the minimum variance estimate of $\bar{y}_I$ does not imply that $\hat{y}_I$ is the minimum variance estimate of η [6]. For target tracking, an estimate of the variance $\sigma^2_{\hat{y}_I}$ is found by setting $\eta = y_I$ and $SNR = Y_N - 1$ in p, resulting in

$$\hat{\sigma}^2_{\hat{y}_I} = \frac{1}{2NY_N}\left[\frac{\sigma_d^2}{\sigma_S^2}\left(1 - \frac{\rho^2}{Y_N}\right) + \left(1 - \frac{1}{Y_N}\right)\hat{y}_I\left(\hat{y}_I - 2\rho\sigma_d\sigma_S^{-1}\right)\right] \tag{18.77}$$

Since the y_{Ik} are Gaussian, $\sigma^2_{\hat{y}_I}$ is the conditional CRLB for $\bar{y}_I$ given $\{SNR_{\text{obs}_k}\}_{k=1}^N$ The term *conditional* here is used to denote the fact that the CRLB is developed with the amplitude-conditioned PDF. While $\hat{\sigma}^2_{\hat{y}_I}$ provides the variance of $\hat{y}_I$ for real-time or actual tracking, $\sigma^2_{\hat{y}_I}$ cannot be used for performance prediction because it is a function of $\{SNR_{\text{obs}_k}\}_{k=1}^N$, which are measured quantities. The modified Cramèr-Rao lower bound (MCRLB) [18], while somewhat looser than the CRLB, can be used for performance prediction. The MCRLB of $\bar{y}_I$ is given by

$$\sigma^2_{\bar{y}_I} \geq J(\bar{y}_I) = \frac{p}{2N(SNR + 1)} \tag{18.78}$$

18.9.2.2 Multiple Unresolved Targets

Conventional monopulse processing is based on the assumption that each observation includes a single resolved object. When measurements of two closely spaced objects are made and conventional monopulse processing is employed, the resulting AOA measurement may not reflect the existence of two targets. Since the position and velocity estimates of a target determine the association of any subsequent measurements to the target, failure to detect the presence of the interference of a second target and address it in the DOA estimation can be catastrophic to the performance of the tracking algorithm. For two unresolved Rayleigh targets, the in-phase and quadrature parts of the sum (s_I and s_Q) and (d_I and d_Q) difference signals are given by [19]

$$\begin{aligned} s_I &= \alpha_1\cos\phi_1 + \alpha_2\cos\phi_2 + w_{sI}, & s_Q &= \alpha_1\sin\phi_1 + \alpha_2\sin\phi_2 + w_{sQ} \\ d_I &= \alpha_1\eta_1\cos\phi_1 + \alpha_2\eta_2\cos\phi_2 + w_{dI}, & d_Q &= \alpha_1\eta_1\sin\phi_1 + \alpha_2\eta_2\sin\phi_2 + w_{dQ} \end{aligned} \tag{18.79}$$

where η_i is the DOA parameter for target i. With SNR_i denoting the average SNR for target i, the joint PDF of the in-phase and quadrature parts of the monopulse ratio for

uncorrelated receiver errors is again given by equation (18.73), but now with

$$p_{y_I}(y_I|SNR_{\text{obs}}) = \text{N}\left(\frac{SNR_1\eta_1 + SNR_2\eta_2}{SNR_1 + SNR_2 + 1}, \frac{\kappa}{2SNR_0}\right)$$

$$p_{y_Q}(y_Q|SNR_{\text{obs}}) = \text{N}\left(0, \frac{q\kappa}{2SNR_0}\right). \tag{18.80}$$

$$\kappa = \left[\frac{\sigma_d^2}{\sigma_s^2} + \frac{SNR_1\eta_1^2 + SNR_2\eta_2^2 + SNR_1SNR_2(\eta_1 - \eta_2)^2}{SNR_1 + SNR_2 + 1}\right]$$

Thus, y_I and y_Q are conditionally Gaussian, independent random variables. Note that equation (18.80) shows that the mean of y_I is a power or energy weighted average of the DOAs of the two targets. With $\bar{y}_I$ denoting the mean of y_I given SNR_0, the ML estimate of $\bar{y}_I$ for N independent pulses is given by equation (18.75). Since the y_{Ik} are Gaussian random variables, $\hat{y}_I$ is the minimum variance estimate of $\bar{y}_I$ and a Gaussian random variable with variance given by

$$\sigma_{\hat{y}_I}^2 = \frac{\kappa}{2NY_N} \tag{18.81}$$

The MCRLB of $\bar{y}_I$ is given by

$$\sigma_{\bar{y}_I}^2 \geq J(\bar{y}_I) = \frac{\kappa}{2N(SNR_1 + SNR_2 + 1)} \tag{18.82}$$

Figure 18-19 gives a comparison of the MCRLBs of $\bar{y}_I$ for a single target and two unresolved, equal-amplitude targets versus the total SNR in a single frequency (i.e., $N = 1$). To obtain $\bar{y}_I = 0$ in both cases, the single target was set at the antenna boresight, and the two targets were situated symmetrically about the boresight (i.e., $\eta_1 = -\eta_2$) and separated by one-half of a beamwidth by setting $\eta_1 = 0.4$ for $k_m = 1.6$. Figure 18-19 shows that a total SNR of 14 dB gives a MCRLB of 0.02 for the single-target case and 0.095 for the two-target case. This figure also shows that doubling the energy in a single-frequency waveform to obtain a total SNR of 17 dB gives an MCRLB of 0.01 for the single-target case and 0.09 for the two-target case. Thus, doubling the energy in a single-frequency pulse gives only a

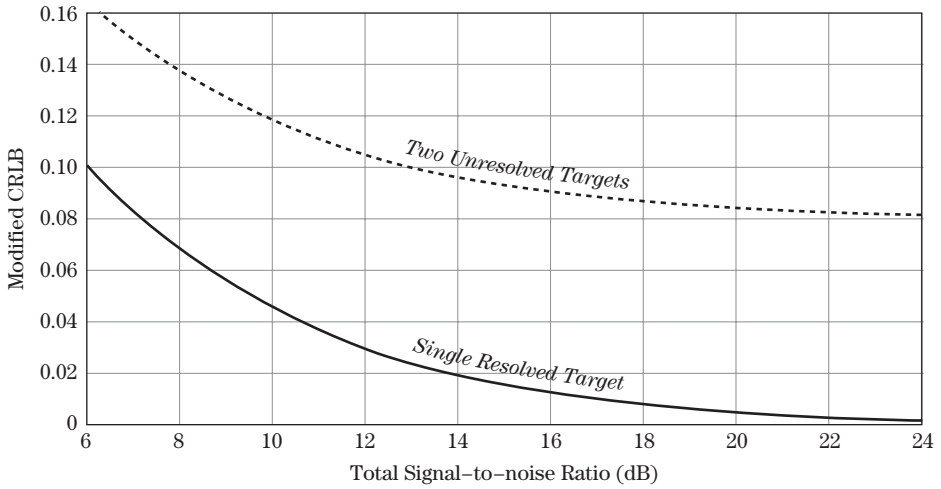

FIGURE 18-19 ■ MCRLBs of $\bar{y}_I$ for a single pulse and single target at the boresight and two targets separated by one-half beamwidth and symmetric about the boresight.

small reduction in the MCRLB for the two-target case. However, if the energy in the pulse is doubled and a second frequency is added so that two independent observations of the unresolved targets are obtained, the MCRLB would be reduced by about 50 percent because the errors are Gaussian (not shown in figure). Therefore, frequency agility is critical to improving the monopulse angle estimation when two unresolved targets are present.

The failure to detect the presence of the interference of a second target can be catastrophic to the performance of the tracking algorithm. A *generalized likelihood ratio test* (GLRT) for detection of the presence of unresolved Rayleigh targets is developed in [3]. Waveform design and antenna boresight pointing for AOA estimation of two unresolved Rayleigh targets with a monopulse radar is addressed further in [19–21].

18.10 COORDINATE SYSTEMS

A radar system measures target position in spherical coordinates relative to the boresight of the radar antenna: range, R, azimuth angle, θ, and elevation angle, ϕ. These two angle coordinates are measured in orthogonal planes in a coordinate system centered on the antenna. If the x direction is the "horizontal" dimension of the antenna, the y direction is the "vertical" dimension of the antenna, and the z dimension is the normal to the antenna face (the boresight direction in a mechanically-scanned antenna), then elevation is measured in the vertical y-z plane containing the radar boresight, while azimuth is measured in the horizontal x-z plane containing the boresight. The measurement errors in these dimensions are generally independent of one another.

Frequently it is the case that it is desirable to track a target in a different coordinate system, typically a Cartesian (x-y-z) system centered at the radar platform or some other convenient reference point. The transformation from the spherical measurement coordinates back to antenna-centered Cartesian coordinates with the same origin is given by (18.83) and illustrated in Figure 18-20.

$$\begin{aligned} x &= R\cos\theta\sin\phi \\ y &= R\sin\theta\sin\phi \\ z &= R\cos\theta \end{aligned} \tag{18.83}$$

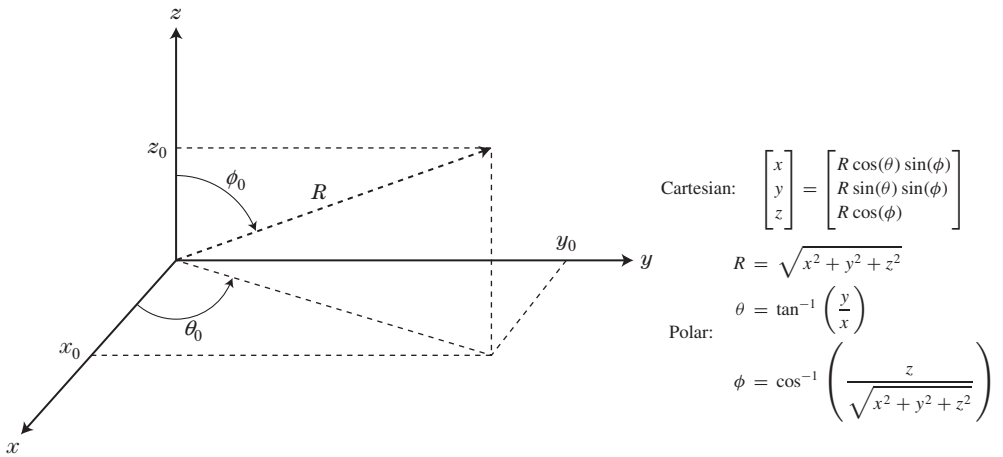

FIGURE 18-20 ■ Spherical and Cartesian representations of a three-dimensional vector.

Equation (18.83) shows that measurement errors in Cartesian coordinates are a nonlinear combination of the spherical coordinate errors. Consequently, the errors in the three Cartesian coordinates are *coupled*: the error in x is not independent of the error in y and so forth. This complicates the design and analysis of optimal tracking algorithms [22]. In practice, the transformation of the uncertainty model in the measurement frame to the track filter reference frame is typically accomplished by linearizing the model in equation (18.83) at the current estimates of R, θ, and φ.

The antenna-centered coordinates can in turn be rotated and translated into alternative Cartesian systems, for instance into coordinates aligned with the platform flight path, or to East-North-Up coordinates. Coordinate systems and coordinate conversion are a major topic in track filtering and are addressed further in Chapter 19.

18.11 FURTHER READING

Additional material and alternative presentations on radar measurement accuracy may be found in several sources. A description of number of practical approaches in radar measurement can be found in Barton and Ward's handbook [6]. Peebles [4] and Raemer [23] provide extensive theoretical results and derivations in radar measurement theory. A good introduction to radar system design and performance analysis is provided by the classic text [24]. Detailed background on the theory of measurement in the presence of noise is provided in the well-known book [25]. A popular forum for publication of current research in this area is the *IEEE Transactions on Aerospace Systems*.

18.12 REFERENCES

[1] Richards, M.A., *Fundamentals of Radar Signal Processing*, McGraw-Hill, New York, 2005.

[2] Blair, W.D., and Keel, B.M., "Radar Systems Modeling for Target Tracking," in *Multitarget-Multisensor Tracking: Advanced and Applications, Vol. III*, Ed. Y. Bar-Shalom and W.D. Blair, Artech House, Dedham, MA, 2000.

[3] Kay, S.M., *Fundamentals of Statistical Signal Processing, Vol. 1: Estimation Theory*, Prentice-Hall, Upper Saddle River, NJ, 1993.

[4] Peebles Jr., P.Z., *Radar Principles*, Wiley, New York, 1998.

[5] Levanon, N., *Radar Principles*, Wiley, New York, 1988.

[6] Barton, D.K., and Ward, H.R., *Handbook of Radar Measurement*, Artech House, Dedham, MA, 1984.

[7] Trunk, G.V., "Range Resolution of Targets Using Automatic Detectors," *IEEE Trans. Aerospace and Electronic Systems*, vol. AES-14, no. 5, pp. 750–755, Sept. 1978.

[8] Trunk, G.V., "Range Resolution of Targets," *IEEE Trans. Aerospace and Electronic Systems*, vol. AES-20, no. 6, pp. 789–797, Nov. 1984.

[9] Cook, C.E., and Bernfeld, M., *Radar Signals: An Introduction to Theory and Application*, Artech House, Norwood, MA, 1993.

[10] Jacobsen, E., and Kootsookos, P., "Fast Accurate Frequency Estimators," *IEEE Signal Processing Magazine*, pp. 123–125, May 2007.

[11] Doviak, R.J., and Zurnic, D.S., *Doppler Radar and Weather Observations*, 2d ed., Academic Press, San Diego, 1993.

[12] Blair, W.D., and Brandt-Pearce, M., "Estimation and Discrimination for Swerling Targets," *Proceedings Twenty-Eighth Southeastern Symposium on System Theory, 1996*, pp. 280–284, March 31–April 2, 1996.

[13] Sherman, S.M., *Monopulse Principles and Techniques*, Artech House, Dedham, MA, 1984.

[14] Galati, G., and Struder, F.A., "Angular Accuracy of the Binary Moving Window Radar Detector," *IEEE Trans. Aerospace and Electronic Systems*, vol. AES-18, no. 4, pp. 416–422, July 1982.

[15] Galati, G., and Struder, F.A., "Maximum Likelihood Azimuth Estimation Applied to SSR/IFF Systems," *IEEE Trans. Aerospace and Electronic Systems*, vol. AES-26, no. 1, pp. 27–43, Jan. 1990.

[16] Swerling, P., "Maximum Angular Accuracy of a Pulsed Search Radar," *Proc. of the IRE*, vol. 44, pp. 1145–1155, Sept. 1956.

[17] Seifer, A.D., "Monopulse-Radar Angle Measurement in Noise," *IEEE Trans. Aerospace and Electronic Systems*, vol. AES-30, pp. 950–957, July 1994.

[18] Gini, F., Reggiannini, R., and Mengali, U., "The Modified Cramer-Rao Bound in Vector Parameter Estimation," *IEEE Trans. on Communications*, vol. 46, no. 1, pp. 52–60, Jan. 1998.

[19] Blair, W.D., and Brandt-Pearce, M., "Monopulse DOA Estimation of Two Unresolved Rayleigh Targets," *IEEE Trans. Aerospace and Electronic Systems*, vol. AES-37, no. 2, pp. 452–469, Apr. 2001.

[20] Willett, P.D., Blair, W.D., and Zhang, X., "The Multitarget Monopulse CRLB for Matched Filter Samples," *IEEE Trans. Signal Processing*, vol. 55, no. 8, pp. 4183–4198, August 2007.

[21] Zhang, X., Willett, P., and Bar-Shalom, Y., "Monopulse Radar Detection and Localization of Multiple Unresolved Targets via Joint Bin Processing," *IEEE Trans. Signal Processing*, vol. 53, no. 4., pp. 122–1236., Apr. 2005

[22] Brookner, E., *Tracking and Kalman Filtering Made Easy*, John Wiley & Sons, Hoboken, NJ, 1998.

[23] Raemer, H.R., *Radar Systems Principles*, CRC Press, Boca Raton, FL, 1997.

[24] Barton, D.K., *Radar System Analysis and Modeling*, Artech, New York, 2005.

[25] Van Trees, H.L., *Detection, Estimation, and Modulation Theory*, John Wiley & Sons, Inc., New York, 1968.

18.13 | PROBLEMS

1. If every RF power measurement has a calibration uncertainty of 0.1 dB, discuss the relative accuracy of RF path calibration by separately calibrating individual components or doing a single end-to-end calibration.

2. Show that the general centroid estimator in equation (18.35) is unbiased when estimating a fixed parameter in of Gaussian noise. Is this result changed for a power law detector?

3. Show the steps in deriving the CRLB equation (18.23) for estimating a constant in independent Gaussian noise.

4. Find the joint probability density function $p(y_1, \ldots y_N|m)$ for N observations $y_k = m + w_k$ of a constant m in independent Gaussian noise given a particular value of m. Determine the maximum likelihood estimate by solving for the argument of $p(y_1, \ldots y_N|m)$ that maximizes the joint probability function. Determine if the maximum likelihood estimate is biased.

5. Derive the CRLB for estimating the RCS for Swerling 2 target in the presence of independent Gaussian noise using the distribution for the measured power given in equation (18.61).

6. For problem 4, show that the maximum likelihood estimator for the signal power is the sample mean.

7. Plot the CRLB of the weight sums of N monopulse ratios for a single versus the various parameters in equation (18.78). Comment on the effects of parameters. For an ideal monopulse system, what would these parameter values be and what would the CRLB be?

8. What is the minimum SNR required in a 40 MHz bandwidth LFM radar to ensure a single-pulse range precision of 30 m?

9. Repeat problem 4 for an unmodulated CW pulse.

10. What is the minimum SNR required for an unbiased phase estimator must produce a minimum error of 10 deg. for $N = 1$ and $N = 10$ pulses?

11. What is the value of the CRLB for frequency estimation for a radar with an SNR = 20 dB, a pulse length of 10 μs, and $N = 1$ pulse? What is the value for $N = 20$ pulses?

12. Compute the RMS bandwidth of (a) a CW pulse with a rectangular envelop, and (b) an LFM chirp. For part (b), assume that the frequency spectrum of the chirp is rectangular. What are the implications of the signal modulation bandwidth on the bound on time-delay measurement precision?

13. Compute the RMS time duration of (a) a rectangular pulse, (b) a triangular pulse, and (c) half cosine pulse envelope shape. What are the implications of the pulse shape on the bound on frequency measurement precision?

14. Derive equations (18.26) and (18.27) assuming the signal *mean time duration* $\bar{\tau}$ and *mean bandwidth* $\bar{B}$ are zero where

$$\bar{\tau} = \frac{\int_{-\infty}^{\infty} t|s(t)|^2 dt}{\int_{-\infty}^{\infty} |s(t)|^2 dt} \qquad \bar{B} = \frac{\int_{-\infty}^{\infty} 2\pi f|S(f)|^2 df}{\int_{-\infty}^{\infty} |S(f)|^2 df}$$